

Report to be submitted to ÅForsk foundation

(Project number: 20-412)

Multi-functional sustainable pulp-based fabric composites for interior applications: Manufacturing, modelling and testing

The report was prepared by Pooria Khalili

Email: Pooria.khalili@hb.se; Pooria.khalili@gmail.com Office number: E804

Phone number 033-435 5959

Mobile: 0790-662525

HÖGSKOLAN I BORÅS

S-501 90 BORÅS

SVERIGE

CONTENTS

| | |
|---|----|
| Publication lists | 3 |
| Impregnation behaviour of regenerated cellulose fabric Elium® composite: experiment, simulation and analytical solution | 5 |
| Summary | 5 |
| 1. Introduction | 6 |
| 2. Methodology..... | 8 |
| 2.1. Materials..... | 8 |
| 2.2. Permeability measurements | 8 |
| 2.3. Resin infusion | 9 |
| 2.4. Simulation and analytical formulation of composite part | 10 |
| 3. Results and discussions..... | 10 |
| 3.1. Permeability measurements | 10 |
| 3.2. Resin infusion data | 12 |
| 3.3. Optimization of permeability using PAM-RTM and process simulation (PAM-RTM and myRTM).... | 13 |
| 3.4. Analytical solution for filling time | 16 |
| 4. Conclusions | 17 |
| Acknowledgments..... | 18 |
| References | 18 |
| Fabrication, mechanical testing and structural simulation of regenerated cellulose fabric Elium® thermoplastic composite system | 22 |
| Summary | 22 |
| 1. Introduction | 23 |
| 2. Materials and Methods..... | 25 |
| 2.1. Materials..... | 25 |
| 2.2. Processing..... | 25 |
| 2.3. Characterization | 26 |
| 2.3.1. Flexural test..... | 26 |
| 2.3.2. Tensile test | 26 |
| 2.3.3. Statistical analysis (ANOVA method)..... | 26 |

| | |
|---|-----------|
| 2.3.4. Scanning Electron Microscope (SEM) test | 26 |
| 2.3.5. Dynamic mechanical analysis (DMA) test | 27 |
| 3. Results and discussion | 27 |
| 3.1. Tensile test analysis | 27 |
| 3.2. Scanning electron microscope (SEM) study of the tensile test..... | 29 |
| 3.3. Flexural test analysis | 29 |
| 3.4. Flexural test simulation and prediction of bending behaviour of a car door panel..... | 32 |
| 4. Conclusions | 38 |
| References | 39 |
| Regenerated Cellulose based fabric thermoplastic composites: Fabrication, mechanical performance, and simulation | 42 |
| Summary | 43 |
| 1. Introduction | 43 |
| 2. Materials and methods..... | 45 |
| 2.1. Materials | 45 |
| 2.2. Film preparation and optimization..... | 45 |
| 2.3. Rayan PP composite and sandwich manufacturing | 46 |
| 3. Characterizations..... | 49 |
| 4. Results..... | 50 |
| 4.1. Bending properties of composites | 50 |
| Modelling the bending properties of balsa wood sandwich bio-composites:..... | 54 |
| 4.2. Tensile behavior of composites..... | 57 |
| 4.3. Impact test analysis | 58 |
| 4.3.1. Force- displacement behaviors..... | 58 |
| 4.3.2. Force-time behaviors | 59 |
| 4.3.3. Energy-time behaviors..... | 60 |
| 4.3.4. Failure and damage modes..... | 61 |
| 4.3.5. Scanning electron microscope (SEM) of fractured surface of the sandwich composite and balsa wood specimens | 61 |
| 4.4. Digital imaging analysis | 62 |
| 5. Conclusions | 64 |
| Acknowledgments..... | 64 |
| References | 64 |
| Mechanical Properties of Bio-Based Sandwich Composites Containing Recycled Polymer Textiles | 68 |

| | |
|--|-----------|
| 1. Introduction | 69 |
| 2. Materials and Methods..... | 72 |
| 2.1. Materials..... | 72 |
| 2.2. Processing | 73 |
| 2.3. Mechanical Properties and Damage Characterisations | 74 |
| 3. Results..... | 76 |
| 3.1. Flexural Properties of Composites | 76 |
| 3.2. Impact Damage Behaviour of Different Composites | 77 |
| 3.2.1. Force-Displacement Response | 81 |
| 3.2.2. Force-Time Behaviours | 82 |
| 3.2.3. Energy-Time Behaviours | 82 |
| 3.2.4. Impact Damage and Failure Modes | 83 |
| 3.3. Tensile Test Analysis of the Composites | 84 |
| 4. Discussion | 84 |
| 5. Conclusions | 86 |
| References | 87 |

Publication lists

1. Impregnation behaviour of regenerated cellulose fabric Elium® composite: experiment, simulation and analytical solution. P Khalili, R Kádár, M Skrifvars, B Blinzler; Journal of Materials Research and Technology. 2021, 10:66-73.

2. Fabrication, mechanical testing and structural simulation of regenerated cellulose fabric Elium® thermoplastic composite system. (Polymers 2021, 13(17), 2969; <https://doi.org/10.3390/polym13172969>)
3. Regenerated cellulose fabric reinforced bio-based polypropylene sandwich composites: fabrication, mechanical performance and analytical modelling (Volume 22, January–February 2023, Pages 3423-3435, doi.org/10.1016/j.jmrt.2022.12.186)
4. Mechanical Properties of Bio-Based Sandwich Composites Containing Recycled Polymer Textiles (Polymers 2023, 15(18), 3815; <https://doi.org/10.3390/polym15183815>)

Chapter 1



Journal of Materials Research and Technology

Volume 10, January–February 2021, Pages 66–73



Original Article

Impregnation behaviour of regenerated cellulose fabric Elium® composite: Experiment, simulation and analytical solution

Pooria Khalili ^{a, b}, , Roland Kádár ^b, Mikael Skrifvars ^a, Brina Blinzler ^b

Impregnation behaviour of regenerated cellulose fabric Elium® composite: experiment, simulation and analytical solution

Summary

Filling time and volume fill prediction of long and complex parts produced using the method of resin infusion is of prominent importance. Fibre volume fraction, reinforcement type and composite laminate thickness significantly affect the manufacturing behaviour. It is crucial to have an estimate of fabrication parameters such as filling time. The PAM-RTM (resin transfer moulding) commercial software package makes it possible to characterize the production parameters in connection with lab scale experiments. In this work, simulation tools demonstrate an accurate prediction of the resin infusion process of pulp-based fabrics and characterization of the dynamic phenomena are verified using the analytical solution for a

simple part. The accurate prediction for fabrication of pulp-based fabric Elium® composite demonstrated here can be beneficial for scaling up the composite part size and production speed. The filling time was accurately predicted until 270 s for the volume fill of 10-100% using the software tool and analytical solution. This proves the rayon fabric processing capabilities as a reinforcement for industry related projects and opens for the possibility of infusion process optimization.

1. Introduction

In the past two decades, the reinforcing potential of lignocellulosic and cellulosic fibres in polymers, in particular thermoplastics, has attracted industry and researchers [1, 2]. Besides natural fibres (NFs), particular consideration has been paid to wood and pulp fibres [3], especially in the countries where this sort of natural resources is abundant such as Sweden. These fibres provide CO₂ neutrality, better disposal and recyclability, reduced abrasion to manufacturing machinery and possess a lower density of 1.5 g/cm³ rather than 2.5 g/cm³ as compared to that of synthetic glass counterpart [4, 5]. Typical NFs lack uniformity. Nonuniformity can reduce their otherwise desirable intrinsic mechanical behaviours. To mitigate this, the individual cellulose fibrils of lignocellulosic fibre (which have the aspect ratios required for efficient reinforcement and are fairly uniform) need to be separated. This has not yet been achieved at a commercial scale and poses substantial practical issues. Besides, since the forest industry is focusing on pulp-based products rather than other natural fibres such as flax, ramie, hemp and jute, in this work we focus on these kinds of products. Rayon, which is a viscose type reinforcement, is produced by regeneration of dissolved cellulose and is used in the form of textile yarns. These yarns have been used as tire cord to reinforce car tires. Their low density and high tenacity lead to good impact resistance and high specific strength [6]. The other significant merit of pulp-based (rayon) fibres over NFs is their repeatable mechanical behaviour in composites as a reinforcement. Natural fibres can exhibit dissimilar properties due to the lack of control based on varying conditions during their growth and their posterior chemical modification.

It was shown that short rayon fibre polypropylene (PP) thermoplastic composite demonstrate comparable mechanical properties with those of glass fibre PP counterparts at 30 wt% of fibre [3]. Tensile strength of rayon-PP composite was recorded 78.7 MPa whereas the glass- PP one displayed a slightly lower value of strength (56.3 MPa). However, the modulus was found to be lower for rayon fiber based composite (2.9 GPa) than that of glass fibre composite (4.1 GPa). This proves the applicability of rayon as a reinforcement. The developed rayon PP composite was used for the fabrication of dashboards and door panels in collaboration with Cordenka and Faurecia interior systems [7].

To explore the processability and reinforcing potential of rayon fabrics in an industrial process like resin infusion, Elium® thermoplastic was selected as the choice of resin. The polymer system used in this work is a novel liquid thermoplastic resin, which possesses low viscosity in order to be processed similar to thermosets [8]. Elium®, which is an acrylic based resin, is polymerized at room temperature and provides mechanical performance similar to commercially used epoxy systems. The incorporation of a peroxide curing agent initiates free radical polymerization and subsequently methyl methacrylate (MMA) monomers react to form poly methyl methacrylate (PMMA) [9]. According to material safety data sheet of the methyl ester of methacrylic acid (CAS:80-62-6), the melting and boiling points are -48 and 100 °C, respectively. The chemical structure of the PMMA resin was previously shown by Bhudolia et al. [10], and the processing temperature is in the range of 20-60 °C.

Vacuum infusion (VI) or resin infusion is widely utilized for its ability to manufacture good-quality large parts. Currently, resin infusion design moulding depends to a great extent on user experience [11]. Hence, in order to cut costs and increase the speed and consistency of production, prediction of the vacuum process in the mould design plays a key role. Commercial Finite Element Method (FEM) software tools can be used to simulate the infusion process of fibre reinforced composites, however, some features of these software programs have minor effect on the infusion processes. Hence, these programs are rarely used in practice, especially at medium and small sized enterprises. Furthermore, these software licenses are costly and detailed material data are unavailable [12]. PAM-RTM (resin transfer moulding) software package uses FE analysis to predict the resin flow front. It allows optimization of outlet and inlet locations to ensure the complete impregnation of the laminate part prior to the beginning of the manufacturing campaign [13]. The permeability value depends on the fibre volume fraction or compression level of laminates and type of reinforcement. For reliable manufacturing simulation, accurate permeability values are crucial [14]. PAM-RTM can contribute to both calibrate the permeability values and predict the behaviour of composite processing. In addition, my-RTM uses cellular automata method to physically simulate the process and the approach was first proposed by Neumann et al. [15]. The algorithm used is based on the effect of the individual parameters according to Darcy's law [16] and calculates the state of the distribution of pressure in each cell during resin filling from the pressure difference and also calculates the properties of the cells in the zone at that particular time [17]. Moreover, if the part geometry is simple, an analytical solution can also reduce the cost of experimental production and save lots of time in this regard [18]. The suggested approach is to develop a mathematical solution with minimal characterization of reinforcement. For this purpose, Correia et al. [11] proposed an effective solution by compiling and developing the available formulations from the literature.

In this work, the reinforcing capabilities of bio-based rayon fabrics were investigated in a liquid thermoplastic matrix for resin infusion applications. Production of rayon fibre thermoplastic composites using resin infusion method has not been previously investigated in the scientific literature. Combination of rayon fabric together with Elium® polymer was used for the first time to make a bio-based fibre acrylic based thermoplastic composite. In addition, very few reports were made to measure the permeability of bio-based fibres. Besides, it was probably the first time PAM-RTM was used to calibrate the permeability value in the literature. Two commercial software packages were then used to simulate the resin infusion process and a unified analytical formulation based on substantial assumptions [19-24] was employed. All three methods were revealed to precisely predict the resin behaviour in the preform.

2. Methodology

2.1. Materials

Elium® 150 thermoplastic resin, a two-component system, was supplied by Arkema company, France. Dibenzoyl peroxide was used as curing agent provided by the same company. The viscosity and liquid density of the resin at the room temperature were 0.1 Pa·s and 1.01 g/m³, respectively. The resin is a colourless limpid liquid with a gel time of 30-40 min at 25 °C. 0/90 plain woven rayon fabrics (Cordenka® 700 2440 dtex) were provided by Cordenka company, Obernburg, Germany. The linear density and areal weight were given as 2482 dtex and 442 g/m², respectively. A yarn consists of 1350 filaments, and the yarn counts in the fabric were 24 yarns/cm in the weft and 40 yarns/cm in the wrap. It is worth highlighting that dtex stands for decitex and is the unit to display weight (grams) over 10000 m in textile industry.

2.2. Permeability measurements

Permeability measurements were carried out on the rayon fabrics according to the previously used method i.e. vacuum infusion [25]. The setup was composed of a flat sheet mould, breather, vacuum bag and preform assembled with a central injection point, as illustrated in Figure 1. Three-layer square shaped preform measuring 150 mm side length was placed on the mould, which was coated with a spray release agent beforehand. To ensure an even distribution of pressure at the periphery, a 2.5 cm wide strip of breather cloth was positioned around the perimeter of the fabrics. A layer of vacuum bag was sealed on the whole assembly followed by connecting the resin inlet and outlet. The resin inlet port was placed right in the centre of the preform and rulers were located over the vacuum film to perform the measurements of flow front position along with the digital camera fixed with a stand right over the system. The tests were performed under 1 bar vacuum pressure, and the three layers of fabric were compacted cyclically three times by

releasing the vacuum in the system and applying it again. The injection time and flow front locations were recorded and pictured at different time intervals to allow for calculations of the permeability values.

It was reported that, in order to obtain exact permeability values, two rigid mould halves are required, therefore a correction factor is required for the current setup [11, 25]. Even with an exact mould cavity thickness, due to well-known difficulties involved in the precise permeability measurements [25], the decision was made to use the PAM-RTM software tool to accurately find the permeability value from the initial approximation based on resin infusion setup. In addition, the composite fabrication technique was also resin infusion.

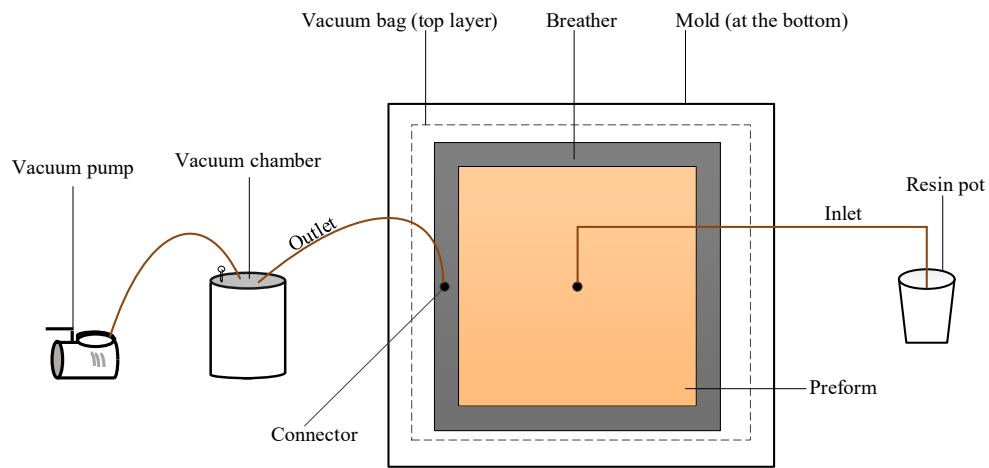


Figure 1. Graphical illustration of experimental setup for the permeability measurement.

2.3. Resin infusion

Since the thermoplastic resin was in the form of liquid, infusion method, which is an open mould technique was selected for composite processing. Closed moulding process such as RTM can be performed as well, if necessary. For the resin infusion test to evaluate the filling time and volume fill percentage, three layers of 0/90 rayon fabric measuring 100×300 mm were cut and then dried in a convection oven for a period of 24 hours at 70°C . They were positioned onto the mould previously surface coated by a layer of release agent (semiprem® monofilm release spray). The testing procedure applied is based on already established protocols [8, 26]. A peel ply was placed on the fabrics and two small pieces of infusion mesh were put on the beginning and the end of the fabric to smoothly initiate and finish the infusion process. Subsequently, two spiral tubes, outlet PVC hose and resin feed PVC hose were attached to the system and the whole assembly was sealed with the aid of gum tape and vacuum bag. A double bagging system was used as

suggested by the resin manufacturer to prevent shrinkage and provide void and detect free composite laminates [8]. Therefore, two layers of vacuum bag were adhered to two strips of gum tape around the perimeter of the mould. The compaction of rayon fabrics was also performed thrice prior to the resin infusion by applying the vacuum and releasing it. The acrylic based resin and dibenzoyl peroxide at the stoichiometric ratio of 100 and 1.5 parts by weight were stirred for three minutes, respectively, then followed by its infusion. The fibre mass and volume fractions were obtained at 55% and 50 %, respectively.

2.4. Simulation and analytical formulation of composite part

The influence of fibre quantity, composite laminate thickness and permeability can be considered for industrial practice process design to simulate the fabrication method. One of the precise process simulation codes developed by ESI group (Paris, France) to predict such behaviour is the commercial PAM-RTM software [13]. myRTM is another program for the simulation of resin transfer moulding (RTM) and resin infusion method. Both software packages contribute to the design of resin infusion and, hence, make efficient component development possible. The limitation of the myRTM software tool is that filling time percentage can be predicted and not the actual times at each step of volume fill unlike the PAM-RTM package.

Analytical formulations of governing equations of vacuum infusion [11] were used in this study to compare the prediction of flow of incompressible resin through compacting porous media with the simulation and experiment. The solution is a very complete development and finalized after compiling several works. The proposed model can quantify the impact of process parameters e.g. fabric lay-up and architecture, outlet and inlet pressures.

3. Results and discussions

3.1. Permeability measurements

In order to calculate the permeability, the plain (0/90) preform was considered orthotropic; however, radial flow front positions along x and y axes corresponding the respective time, which formed a circular shape, Figure 2. (a), were almost the same after three repetitions of the test. This was expected as the properties and flow front are the same along 0 and 90 degree fiber orientations, similar to that of an isotropic material, and the laminate is balanced in plane direction. Therefore, the following equation (1) was selected. Chan et al. [27] and Adams et al. [28] provided a solution for the case of an in-plane (pseudo-) steady state flow of an incompressible fluid which in dimensionless form is:

$$F = \rho_f^2(2\ln\rho_f - 1) = \frac{4 \times K \Delta P t}{\phi \mu R_o^2} \quad (1)$$

where ρ_f is the ratio of the flow front radius (R_f) to the inlet port radius (R_o), and K , ΔP , t , ϕ and μ represent the permeability, the pressure gradient between the outlet gate and the flow front, the elapsed time, the porosity and the resin viscosity, respectively (Table 1). A linear regression through the origin and the data yields a plot of dimensionless F versus time (s), and the line slope can be used to calculate the permeability value (K). Function F represents the relationship between the flow front radius and the elapsed time.

The flow front positions were recorded after 10 seconds such that the resin passed the silicon connector radius (16 mm). Figure 2. (b) shows the mean flow front radius (R_f) at different progressive time and Figure 3 demonstrates the dimensionless function F curve derived from the R_f -time data. It is worth noting that the testing duration was designed to minimize the effect of alteration in resin viscosity due to the curing.

From the manufactured composite part, the required data was obtained to calculate the permeability, K (Table 1). The permeability for the rayon fabric was measured $0.722 \cdot 10^{-10} \text{ m}^2$. Lebrun et al. [25] used the same setup to measure the permeability of flax fibre, absorption paper and glass fibre with a resin viscosity of 0.42 Pa.s. The K values for flax 200 (200 unidirectional text yarn), flax 1000, absorption paper and glass along the x axis (UD direction) were calculated as $0.0498 \cdot 10^{-10}$, $0.0253 \cdot 10^{-10}$, $0.0065 \cdot 10^{-10}$ and $1.0953 \cdot 10^{-10} \text{ m}^2$, respectively. Therefore, the K is higher for glass than rayon fabric investigated, which is expected as synthetic fibres typically possess a higher degree of K .

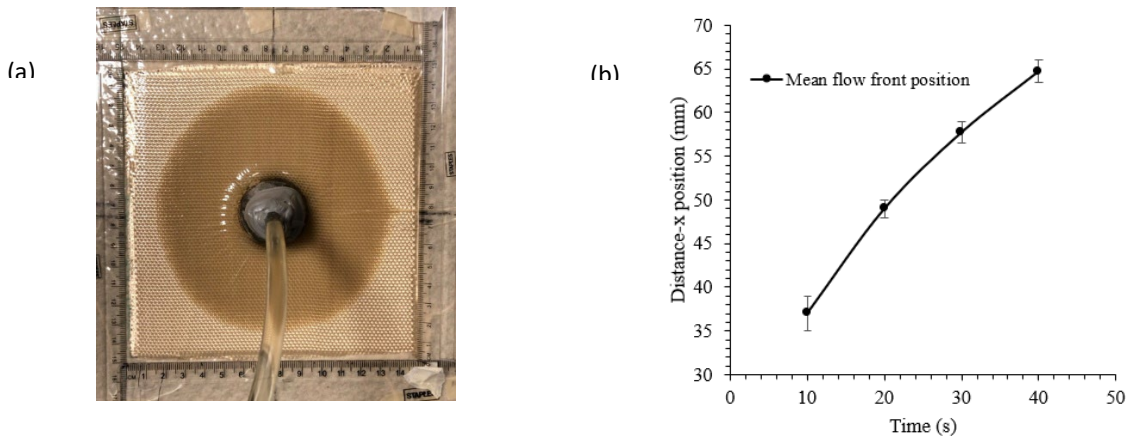


Figure 2. (a) the circular flow front position of resin in the preform in the permeability test after 30 s and (b) mean flow front position from the middle of preform with respect to time.

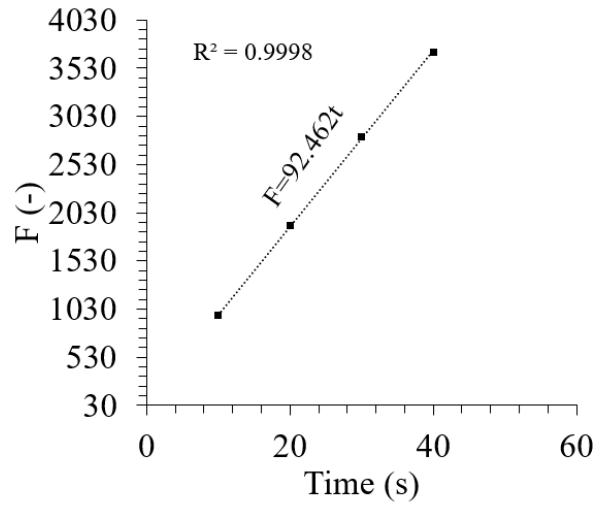


Figure 3. Function F vs. time (s) for the pulp-based fabric.

Table 1. The fitting parameters used to estimate the permeability.

| Description | Symbol | Value | Unit |
|-----------------|--------|--------|------|
| Porosity | Φ | 0.5 | - |
| Vacuum pressure | P | 100000 | Pa |
| Resin viscosity | μ | 0.1 | Pa·s |
| Thickness | T | 1.5 | mm |
| Gate diameter | d | 5 | mm |

This method provides good approximation to calculate the permeability [25] and in the following section the accuracy of the value was validated with the experimental work (composite fabrication). Then, a resin infusion simulation by the PAM-RTM software tool was performed to calibrate the K obtained from the experimental setup.

3.2. Resin infusion data

The infusion time and infused distance (flow front progression) were obtained and the experimental setup and values are shown in Figure 4. The infusion time started as soon as the resin entered the inlet silicon connector (0 s) and the process was considered completed once the resin flow front passed the 300 mm rulers positioned on both sides of the setup. Values of fill time directly depend on the fibre volume fraction

and permeability [11]. As it can be seen from the data, the fill time prolonged at each step when the resin flowed towards the outlet region, and the time versus infused position plots are second order polynomials, which is expected in the vacuum infusion experimental observations.



| Infused distance (mm) | Mean fill time (s) |
|-----------------------|--------------------|
| 0 | 0 |
| 30 | 8 |
| 60 | 14 |
| 90 | 27 |
| 120 | 45 |
| 150 | 68 |
| 180 | 97 |
| 210 | 127 |
| 240 | 165 |
| 270 | 208 |
| 300 | 270 |

Figure 4. Resin infusion setup and the mean data for the infused composite plate.

3.3. Optimization of permeability using PAM-RTM and process simulation (PAM-RTM and myRTM)

Normally, commercial software tools are used to reduce the cost associated with experimental materials and labour, and in this case a resin infusion method was calibrated with PAM-RTM simulation to obtain the exact permeability value without performing RTM fabrication test to measure the permeability. PAM-RTM, a mould filling simulation, works in accordance with two governing equations i.e. Darcy's and continuity equations [29].

Figure 5 displays the PAM-RTM simulations versus experiment plots and it was found that the initial prediction without calibration of permeability resulted in longer filling times for the volume fill percentage of 50 and above. For the initial K-PAM-RTM results, eleven and thirty-one nodes were selected along the width and length for the meshing purpose whereas for initial permeability value with a finer mesh (K-PAMRTM-finer mesh), twenty-one and sixty-one nodes were chosen, respectively. As seen in the behaviour of finer mesh, filling time was slightly closer to the experiment. Therefore, a finer mesh was utilized for the preform to predict the flow front position with the calibrated permeability ($0.85 \text{ e}^{-10} \text{ m}^2$) extracted from the PAM-RTM simulation. Hence, since the behaviour of reinforcement in terms of permeability for the current thickness and resin viscosity was obtained, and that the filling time can precisely be predicted for large and complex shapes using PAM-RTM software tool. The slight increase in

the K value after calibration could be due to the presence of peel ply on the preform in the resin infusion test, which is neglected in the simulation. The simulation results at different volume fill percentages are shown in Figure 6 and the pink colour illustrates the flow front progression. In the following discussions, the absolute accuracy of calibrated permeability would be validated by the prediction of fill time using another software package and analytical solution.

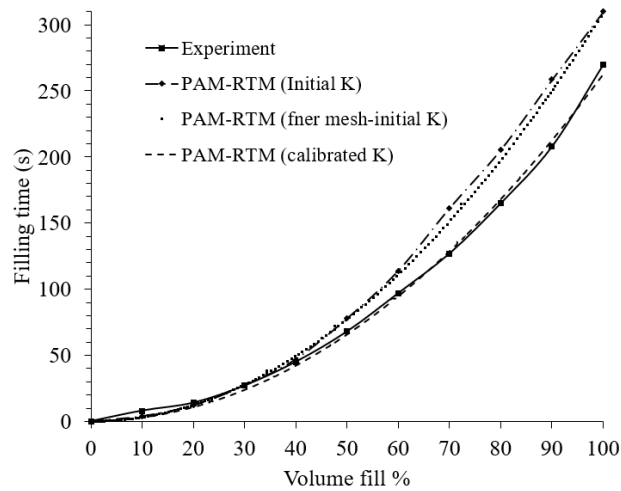


Figure 5. Resin infusion experiment vs. PAM-RTM simulation.

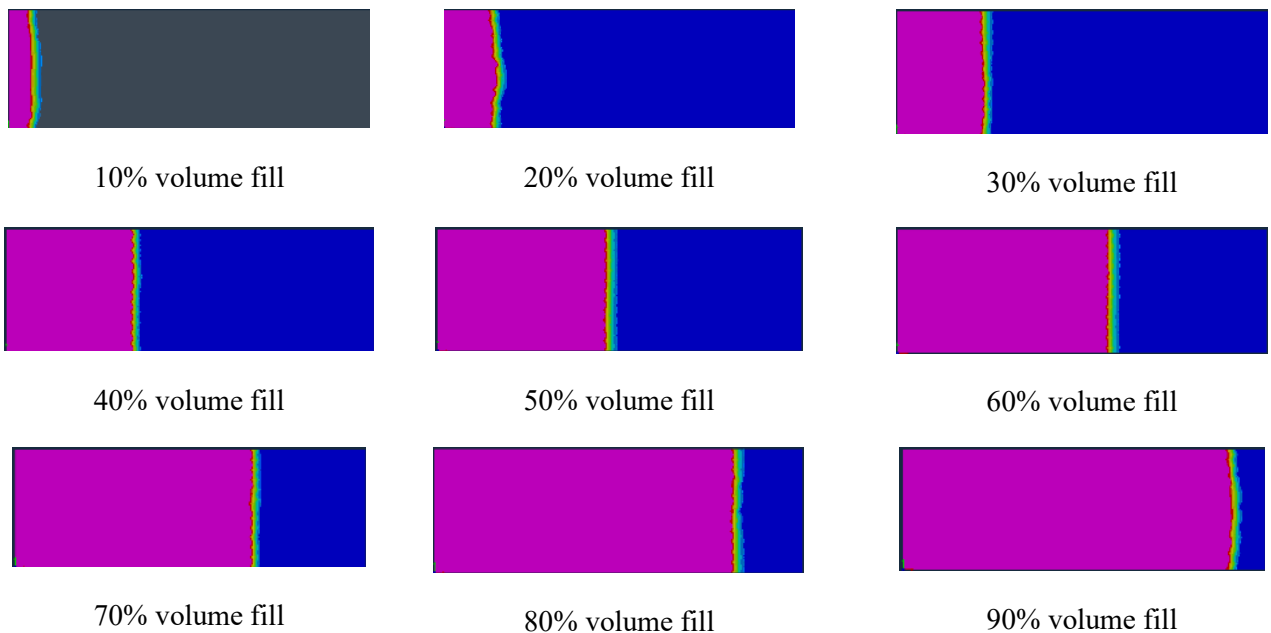


Figure 6. PAMRTM simulation results of rayon fabric composite plate (twenty-one nodes along the width and sixty-one nodes along the length).

For myRTM simulation, the preform was first designed in CATIA V5 and then was imported to the gmsh software tool for meshing before running the myRTM simulation. The program is based on the Cellular Automata principle to predict the resin flow position and is known as a preliminary process design package [12]. Figure 7 shows the filling time percentage and the volume fill percentage of the resin infusion process and myRTM simulation from the beginning state until the end. When the simulation was run with the initial K value, the result did not match well with the experimental work whereas myRTM simulation run with the K value, obtained by PAM-RTM software tool, was found to accurately predict the filling time percentage.

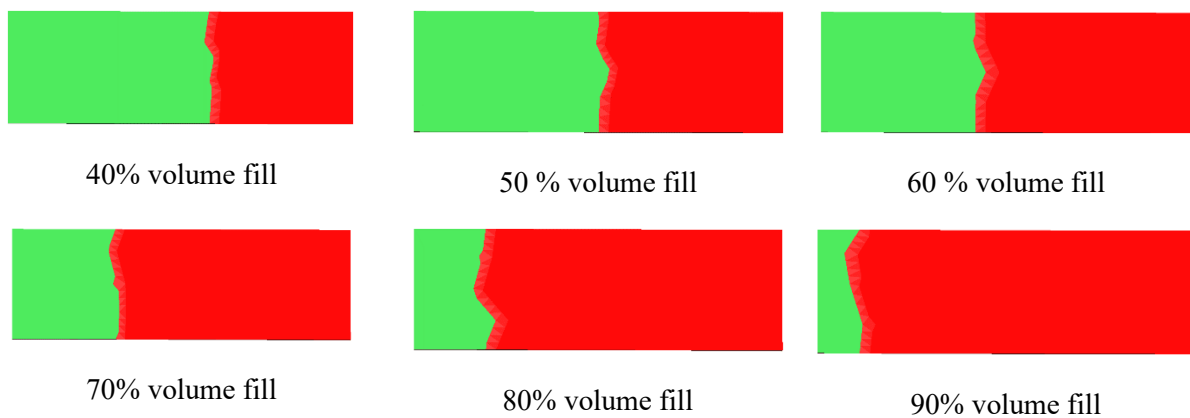


Figure 8 displays the progression of resin from 40 % to 90 % volume fill in the rayon preform during infusion simulated by myRTM software. The software was successfully used in another work to predict the state of the resin in the preform where a bent composite part was manufactured [30].

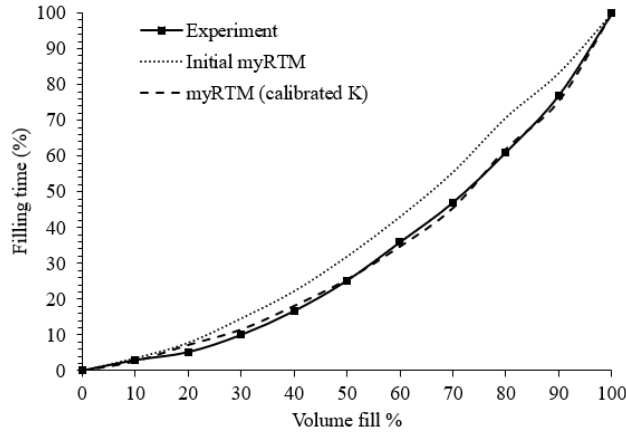


Figure 7. Experimental filling time compared to myRTM simulation of resin infusion process.

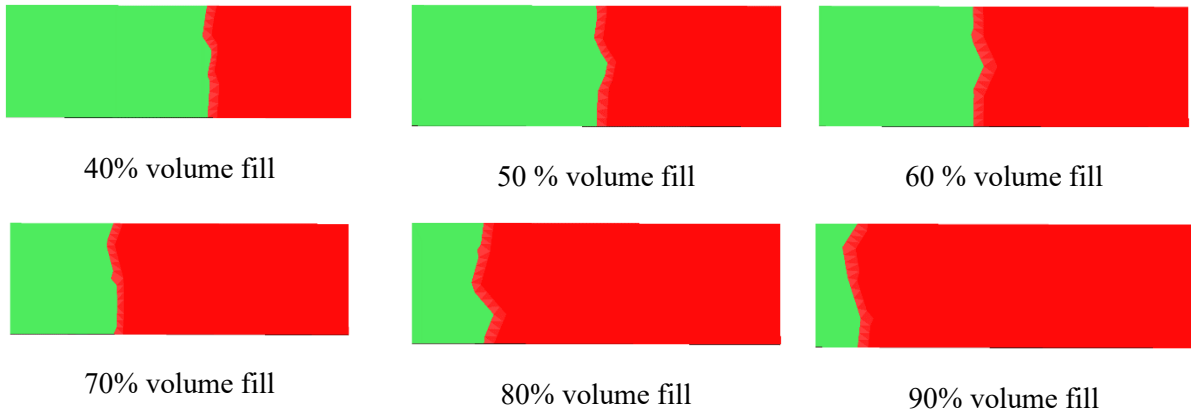


Figure 8. myRTM simulation from 40 %-90% volume fill.

3.4. Analytical solution for filling time

A unified analytical solution was gathered for resin infusion process [11]. Expressing the pressure gradient at the flow front governs progression of flow front and noting fluid pressure as a function of dimensionless flow coordinate (α), which is the ratio of in plane flow direction (x) over the instantaneous flow front location (L) [11], Darcy's law for resin infusion is obtained as

$$\frac{dL(t)}{dt} = \frac{1}{\mu} \left(\frac{K}{\phi} \right)_{\alpha=1} \left[\left(\frac{dP}{d\alpha} \right)_{\alpha=1} \frac{1}{L(t)} \right] \quad (2)$$

where $(\frac{dP}{d\alpha})_{\alpha=1}$, $(K)_{\alpha=1}$ and $(\phi)_{\alpha=1}$ represent the pressure gradient, permeability and porosity at the flow front ($\alpha=1$). The fill time is yielded after integration:

$$t_{infusion} = \frac{\mu}{2} \frac{L^2}{\left(\frac{K}{\phi} \frac{dP}{d\alpha}\right)_{\alpha=1}} \quad (3)$$

The material data available in Table 1 was used to obtain the fill times at different volume fill % from Eq. (3). Figure 9 presents the plots for both experiment and developed analytical solution and it can be found that the prediction is very accurate. The plots of times versus flow front position are second order polynomials [11].

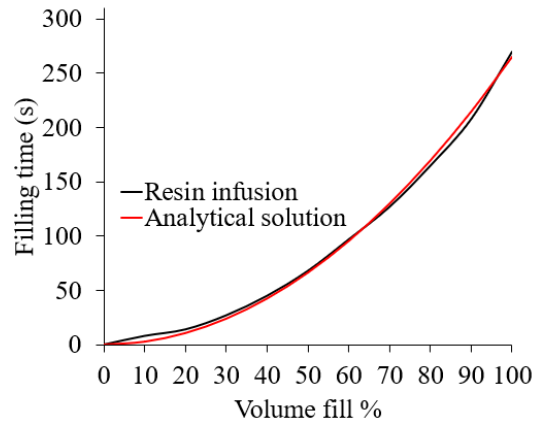


Figure 9. Comparison between experimental filling time and the analytical solution, Eq. (3).

Hence, it was determined that all three means of predicting the flow front position of Elium® resin in the rayon preform (i.e. PAM-RTM, myRTM and analytical formulation) were matching the experimental result. This can ease the initial experimental evaluation of vacuum infusion in particular for long components, and product developers can have an estimation of production process and adjust the parameters e.g. inlet gates and spiral location to control the manufacturing in such a way required.

4. Conclusions

The permeability and resin infusion tests were successfully carried out for rayon fibre reinforced Elium® composites. The required data was obtained and used for simulations and an analytical solution. It was found that PAM-RTM commercial software package is a very beneficial tool for prediction of resin infusion behaviour and calibration of permeability values. Simulation results were compared against the analytical solution and a very good agreement in terms of the prediction of flow front time at different locations along the preform was demonstrated. This demonstrated the potential of simulation and analytical formulations for industrial usage with regards to process optimization and efficiency. Rayon showed its capability to be processed for resin infusion applications with a liquid thermoplastic resin. The wood-based cellulose fibres

are an important resource from the Swedish forest industry which can be used as pulp-based rayon fabrics as bio-based reinforcement material. The combination of permeability and resin infusion experiments together with the PAMRTM simulation for a simple geometry can provide a solid approach to achieve precise permeability values in order to design the processing for complex and large parts. The analytical solution can also be used in such a way to complement and validate the processing design.

In the next step the tensile and flexural performances of this developed composites are compared with other types of natural fibre composites investigated thus far. This demonstrates the potential of replacement of jute and flax fibres with rayon fabrics in countries which have forest industry and can get advantage of their natural resources, in particular in the Nordic region.

Acknowledgments

The financial support for this project is provided by Chalmers Area of Advance: Materials Science and **ÅForsk grant (ref.no. 20-412)**. The work was performed by the support of All Wood Composites Platform at Chalmers University of Technology and the PAM-RTM software was sponsored by ESI group with the support of Dr. Rajab Said, Lotta Modin and Jonas Fredriksson (Gothenburg office, Sweden). Special thanks to Arkema for sponsoring the thermoplastic resin and to Cordenka for sponsoring the rayon fabrics. The authors would like to thank Sreehari Batni Ravindranath and Madhav Bhallamudi for the technical support in the samples' preparation.

References

- [1] Spoljaric S, Genovese A, Shanks RA. Polypropylene–microcrystalline cellulose composites with enhanced compatibility and properties. *Composites Part A: Applied Science and Manufacturing*. 2009;40(6):791-9.
- [2] Bourmaud A, Pimbert S. Investigations on mechanical properties of poly(propylene) and poly(lactic acid) reinforced by miscanthus fibers. *Composites Part A: Applied Science and Manufacturing*. 2008;39(9):1444-54.
- [3] Ganster J, Fink H-P, Pinnow MJCPAAS, Manufacturing. High-tenacity man-made cellulose fibre reinforced thermoplastics–injection moulding compounds with polypropylene and alternative matrices. 2006;37(10):1796-804.

- [4] Khalili P, Liu X, Tshai KY, Rudd C, Yi X, Kong I. Development of fire retardancy of natural fiber composite encouraged by a synergy between zinc borate and ammonium polyphosphate. *Composites Part B: Engineering*. 2019;159:165-72.
- [5] Khalili P, Tshai K, Kong I. Natural fiber reinforced expandable graphite filled composites: Evaluation of the flame retardancy, thermal and mechanical performances. *Composites Part A: Applied Science and Manufacturing*. 2017;100:194-205.
- [6] Skrifvars M, Dhakal H, Zhang Z, Gentilcore J, Åkesson D. Study on the mechanical properties of unsaturated polyester sandwich biocomposites composed of uniaxial warp-knitted and non-woven viscose fabrics. *Composites Part A: Applied Science and Manufacturing*. 2019;121:196-206.
- [7] Ganster J, Erdmann J, Fink H-PJP. Biobased composites. 2013;58(6):423-34.
- [8] Khalili P, Blinzler B, Kádár R, Blomqvist P, Sandinge A, Bisschop R, et al. Ramie fabric Elium® composites with flame retardant coating: Flammability, smoke, viscoelastic and mechanical properties. *Composites Part A: Applied Science and Manufacturing*. 2020;137:105986.
- [9] Van Rijswijk Kv, Bersee H. Reactive processing of textile fiber-reinforced thermoplastic composites—An overview. *Composites Part A: Applied Science and Manufacturing*. 2007;38(3):666-81.
- [10] Bhudolia SK, Perrotey P, Joshi SC. Optimizing Polymer Infusion Process for Thin Ply Textile Composites with Novel Matrix System. 2017;10(3):293.
- [11] Correia N, Robitaille F, Long A, Rudd C, Šimáček P, Advani SJCPAAS, et al. Analysis of the vacuum infusion moulding process: I. Analytical formulation. 2005;36(12):1645-56.
- [12] Barandun G, Henne M, Giger E, Arbter R. MyRTM: An Approach for the simulation of resin transfer moulding (RTM) processes based on cellular automata. *Proceedings of the 6th European Congress on Computational Methods in Applied Sciences and Engineering (ECCOMAS 2012)*, Vienna, Austria 2012. p. 10-4.
- [13] Poodts E, Minak G, Dolcini E, Donati L. FE analysis and production experience of a sandwich structure component manufactured by means of vacuum assisted resin infusion process. *Composites Part B: Engineering*. 2013;53:179-86.
- [14] Drapier S, Monatte J, Elbouazzaoui O, Henrat PJCPAAS, Manufacturing. Characterization of transient through-thickness permeabilities of non crimp new concept (NC2) multiaxial fabrics. 2005;36(7):877-92.
- [15] Von Neumann J, Burks AWJIToNN. Theory of self-reproducing automata. 1966;5(1):3-14.

- [16] Darcy HPG. Les Fontaines publiques de la ville de Dijon. Exposition et application des principes à suivre et des formules à employer dans les questions de distribution d'eau, etc: V. Dalamont; 1856.
- [17] Henne M, Barandun G. Simulation of LCM processes using cellular automats. The 10th International Conference on Flow Processes in Composite Materials (FPCM10). p. 11-5.
- [18] Goncharova G, Cosson B, Deléglise Lagardère M. Analytical modeling of composite manufacturing by vacuum assisted infusion with minimal experimental characterization of random fabrics. *Journal of Materials Processing Technology*. 2015;219:173-80.
- [19] Scheidegger AEJSS. The physics of flow through porous media. 1958;86(6):355.
- [20] De Boer R. *Theory of porous media: highlights in historical development and current state*: Springer Science & Business Media; 2012.
- [21] Biot MAJJoap. General theory of three-dimensional consolidation. 1941;12(2):155-64.
- [22] Gebart BRJJocm. Permeability of unidirectional reinforcements for RTM. 1992;26(8):1100-33.
- [23] Gutowski T, Dillon GJAcM. *The elastic deformation of fiber bundles*. Wiley, New York; 1997. p. 138-9.
- [24] Hammami A, Gebart B. Analysis of the vacuum infusion molding process. *Polymer composites*. 2000;21(1):28-40.
- [25] Lebrun G, Couture A, Laperrière L. Tensile and impregnation behavior of unidirectional hemp/paper/epoxy and flax/paper/epoxy composites. *Composite Structures*. 2013;103:151-60.
- [26] Khalili P, Blinzler B, Kádár R, Bisschop R, Försth M, Blomqvist PJM. Flammability, Smoke, Mechanical Behaviours and Morphology of Flame Retarded Natural Fibre/Elium® Composite. *Materials* 2019;12(17):2648.
- [27] Adams K, Russel W, Rebenfeld LJJoMF. Radial penetration of a viscous liquid into a planar anisotropic porous medium. 1988;14(2):203-15.
- [28] Chan AW, Hwang STJPE, Science. Anisotropic in-plane permeability of fabric media. 1991;31(16):1233-9.
- [29] Kim J-I, Hwang Y-T, Choi K-H, Kim H-J, Kim H-S. Prediction of the vacuum assisted resin transfer molding (VARTM) process considering the directional permeability of sheared woven fabric. *Composite Structures*. 2019;211:236-43.

[30] Makinde OM. Prediction of shape distortions in composite structures: Instituto Tecnológico de Aeronautica; 2018.

Chapter 2

Chapter 2



Submit to this Journal

Review for this Journal

Edit a Special Issue

Article Menu

Article Overview ^

- Abstract

Open Access Article

Fabrication: Mechanical Testing and Structural Simulation of Regenerated Cellulose Fabric Elium[®] Thermoplastic Composite System

by Pooira Khalili ^{1,*} , Mikael Skrifvars ¹ and Ahmet Semih Ertürk ²

¹ Swedish Centre for Resource Recovery, University of Borås, 510 90 Borås, Sweden

² Department of Industrial and Materials Science, Chalmers University of Technology, 412 96 Gothenburg, Sweden

* Author to whom correspondence should be addressed.

Academic Editor: Carmelo Corsaro

Polymers **2021**, *13*(17), 2969; <https://doi.org/10.3390/polym13172969>

Fabrication, mechanical testing and structural simulation of regenerated cellulose fabric Elium[®] thermoplastic composite system

Summary

Regenerated cellulose fibers are an important part of the forest industry and they can be used in the form of fabrics as reinforcement materials. Similar to natural fibers (NFs) such as flax, hemp and jute widely used in automotive industry, these fibers possess good potential to be used for semi structural applications. In

this work the mechanical properties of regenerated cellulose fabric reinforced poly methyl methacrylate (PMMA) (Elium®) composite were investigated and compared with those of natural fiber composite counterparts. The developed composite demonstrated higher tensile strength and ductility as well as comparable flexural properties with those of NF reinforced epoxy and Elium® composite systems whereas the Young's modulus was lower. Glass transition temperature demonstrated a competitive value (107.7 °C) to that of other NF composites. Then, the behavior of the bio-composite under bending loading was simulated and the materials model was used to simulate the behavior of a car door panel in a flexural scenario. The modelling can contribute to predict the structural behavior of the bio-based thermoplastic composite for secondary applications, which is the aim of this work. Finite element simulations were performed to assess the deflection and force transfer mechanism for the car door interior.

Keywords: regenerated cellulose fiber; thermoplastic resin; Finite element (FE); mechanical performance

1. Introduction

Pulp, paper and wood fibers along with plant fibers for instance jute, flax and hemp have attracted considerable attention in the past two decades. It has continually been appealing to utilize bio-based/natural fibers rather than synthetic ones, in particular glass fibers (GF) as the predominating reinforcing element [1].

Regenerated cellulose (rayon) fibers have been demonstrated to present substantial promise as reinforcements for thermoplastics [1-3]. Regenerated cellulose fibers possess unique characteristics in the sense that they offer the merit of both natural (NF) and synthetic fibers. These include on the one hand low density, CO₂ neutrality [4], non-abrasiveness to processing equipment [4] and biodegradability [5] of NFs, and on the other hand the physical, mechanical and uniform morphological properties of synthetic ones. Rayon is manufactured by regeneration of dissolved cellulose and is utilised in the textile yarn forms. Due to their high tenacity, which leads to good impact resistance, high specific strength and low density (~1.5 g/cm³), rayon yarns have been utilised to reinforce car tires as tire cord [6].

Several articles have been published on the topic spanning a diversity of manufacturing routes and combinations of rayon fiber and matrices. Primarily, the works have been performed to produce short fiber thermoplastic composites using the melt-mixing coupled with injection molding followed by solvent impregnation or pultrusion [1, 3, 7] and compression molding for continuous fiber composites. Polypropylene (PP) seems to have been the most attractive choice of polymer for regenerated cellulose fiber reinforced composites thus far.

It was reported that short rayon fiber PP composites demonstrate comparable mechanical performance to those of GF PP materials at the same fiber mass fraction (30 wt%) [1]. Although the tensile modulus was lower for regenerated cellulose PP composite (2.9 GPa) than that of GF counterpart (4.1 GPa), the strength was measured 78.7 MPa, which showed 40% increase than that of GF PP composite. This proves the potential of this type of bio-based fiber as a reinforcement in the composite systems. The resulting rayon PP composite was utilised in the production of door panels and dashboards by Faurecia interior systems and Cordenka [7]. In the automotive industry, it was revealed that rayon-based composites offer excellent mechanical performance reaching and partially surpassing the level of GF ones [8,9]. In comparison with NF counterparts, regenerated fiber composites display significant enhancement in strength and impact properties [7] whilst stiffness can easily be improved by the incorporation of NFs at a good level [10].

For semi structural applications, these sorts of fibers can be used in the form of fabric, and the woven structure of the reinforcement can further enhance the properties of the developed composite. It is customary to use a type of liquid thermoset to develop a composite based on textile reinforcements. Thermosets, due to their high mechanical behaviour, are used in high-performance applications. On the other hand, thermoplastics are appealing to the manufacturers as they provide high impact tolerance [11], good vibration dampening capacities [12], recyclability [11], post-manufacturing formability [13] and some with eco-friendly contents [14]. A novel thermoplastic resin (Elium®) has been developed by Arkema Chemicals which enables the process of composites at room temperature (as a result, less energy-intensive thermoplastic polymer relative to that of other ones) and offers similar mechanical properties to epoxy-based systems. This manufacturing condition contributes to prevent degrading the performance of the bio-based fiber, which is generally caused by high processing temperature of thermoplastics. Resin infusion and resin transfer molding (RTM) can be employed to polymerise the fiber reinforced Elium® part at ambient temperature. The incorporation of a peroxide curing agent into the monomer (methyl methacrylate (MMA) initiates free radical polymerization, which subsequently reacts to form poly methyl methacrylate (PMMA) polymer [15,16]. It is worth noting that higher bio-based fiber mass fraction can be obtained in the composites when using hot compression or resin infusion methods than that of injection molding technique. This can be a crucial point which needs to be taken into account when the presence of maximum fiber content in the part is important [17-19].

In this work the reinforcing capabilities of rayon fabric in the liquid thermoplastic resin were investigated. The mechanical performance and glass transition temperature of the resulting composite were compared with those of other bio-based and NF (jute and ramie) thermoset/thermoplastic composite systems. Very few studies reported the tensile, flexural and viscoelastic behaviour of rayon fabric Elium® composite (the

combination of a regenerated cellulose cellulose fabric and Elium®) and were found to show the potential of this type of bio-based fabric composite for secondary applications. Scanning Electron Microscope (SEM) analysis was performed to investigate the mode of fracture after the tensile test. Rayon fabric Elium® composite produced using resin infusion (RI) method, which is typically employed in fabric reinforced thermoset composites. Rayon and Elium® were used for the first time to make a bio-based fabric thermoplastic composite using RI method, to the best of authors knowledge. A finite element (FE) model was developed, and the model indicated to be capable of predicting the structural performance of the regenerated cellulose Elium® composite panel. The bending performance of the bio-based composite was modelled with a polynomial function and the materials model was applied to the FE (ABAQUS) software for the calibration and validation of the bent rectangular sample. Subsequently, the same materials model was assigned to a door car (interior) panel, and then the bending deformation, deflection and reaction forces were predicted. This kind of simulation has not been extensively carried out for bio-based composites.

2. Materials and Methods

2.1. Materials

0/90 plain-woven rayon fabrics with the nominal weight of 442 g/m² were provided by Cordenka GmbH, Obernburg, Germany, and had the linear density and breaking force of 2485 dtex and 796 MPa, respectively. Elium® 150 polymer was supplied by Arkema company, Colombes, France. The viscosity and liquid density were 0.1 Pa.s and 1.01 g/m³, respectively, and dibenzoyl peroxide was used as curing agent.

2.2. Processing

The composite plates measuring 100 mm × 300 mm were produced using resin infusion technique [2]. Three layers of rayon fabrics were dried in a convection oven for 24 h at 70 °C prior to the start of infusion. They were placed on a surface coated mold, followed by positioning a layer of peel ply on the fibers. Spiral tube, silicon connectors, outlet PVC hose and resin feed PVC hose were connected to the assembly. Subsequently, the whole system was sealed with the aid of gum tape and vacuum bag. As recommended by the manufacturer, to avoid shrinkage of composites double bagging was employed to seal the assembly. Then, compaction of fabrics was performed to enhance the fiber fraction in the resulting composite; the vacuum was applied in the vacuum bag and released thrice for this purpose. The sealed assembly was left for 10 min to ensure a leakage free system. The resin and dibenzoyl peroxide at a stoichiometric ratio of 100 to 1.5 parts by weight were stirred manually for three min and the mix was degassed for three min to eliminate the trapped gases. The resin infusion was carried out and the part was

left to cure for 24 h at the ambient temperature. The composite plates possessing about 1.5 mm thickness were demolded and the fiber volume and mass fractions were 50% and 55%, respectively. The infusion process lasted 4.5 min for three layers of fabrics at the mentioned dimension. The resulting composites were cut into specified sample dimensions with the aid of laser cutting equipment for tests.

2.3. Characterization

2.3.1. Flexural test

The bending performance of rayon fiber reinforced composite laminate was studied using a Tinius Olsen H10KT universal testing instrument, Horsham, USA, in accordance with BS EN ISO 14125. Five rectangular specimens of the dimension of 80 mm × 20 mm (length × width) with a span length of 64 mm were characterized. The cross-head speed and the load-cell of test machine were fixed at 5 mm/min and 5 kN, respectively. For all types of tests in this work, the samples were conditioned for 24 h in a humidity chamber with the temperature of 23 °C and the humidity of 50% before the characterizations.

2.3.2. Tensile test

Tensile properties of rayon fiber reinforced composite laminate were investigated according to BS EN ISO 527 on a Tinius Olsen H10KT universal testing instrument, Horsham, USA, equipped with a 100R mechanical extensometer. Five rectangular specimens measuring 150 mm × 20 mm (length × width) were tested, and both ends of specimens were attached to the tabs of 25 mm length. The load-cell and the cross-head speed were set to 5 kN and 1 mm/min, respectively.

2.3.3. Statistical analysis (ANOVA method)

A one-way statistical analysis was performed by ANOVA method to investigate the variance for the tensile and flexural test results individually. The significant difference between the composites on the strength and modulus was investigated. To evaluate the significance of each property, the P-value parameter was introduced.

2.3.4. Scanning Electron Microscope (SEM) test

The cross-sectional surface of tensile specimens after fracture was investigated using scanning electron microscopy (SEM) equipment. The machine was a FEI Quanta200 ESEM, Oregon, USA, operating an accelerating voltage of 3 kV. The specimens were gold sputtered on a sputter coater Edwards S150B, Perth, UK with the plasma exposition of 60 s in vacuum before the scanning.

2.3.5. Dynamic mechanical analysis (DMA) test

Dynamic mechanical analysis (DMA) tests were carried out with the aid of Rheometrics Solids Analyzer RSA II, (TA Instruments, New Castle, DE), USA. The three-point bending mode was used for the samples previously conditioned for 24 h at 23 °C and 50% humidity in a humidity chamber prior to the testing. The dimension of the rectangular samples was 50 mm × 10 mm, and the heating rate and frequency were set to 5 °C/min and 1 Hz, respectively. The temperature was increased from 30 °C to 170 °C, and subsequently the storage modulus (E') and $\tan \delta$ (loss factor) were measured.

3. Results and discussion

3.1. Tensile test analysis

Tensile tests were performed to study the strength, modulus and elongation at break of the rayon Elium® composite and to compare the respective results with the available natural fiber (NF) composite counterparts.

Incorporation of rayon instead of NF was evidently seen to enhance the strength and toughness of the composites compared to that of natural fiber composites as the breaking point elongated to a much higher value (Table 1) using the same manufacturing technique, as conducted by the authors [20,21]. It was shown that rayon fiber has higher elongation and lower modulus than those of flax fiber [22].

Table 1. Comparative average tensile strength, modulus and elongation at break (EAB) of rayon fiber composite with those of NF counterparts.

| | Tensile strength (MPa) | STD (Strength) | Tensile modulus (GPa) | STD (Modulus) | Elongation at STD (EAB) break (%) | |
|-----------------------------|-------------------------------|-----------------------|------------------------------|----------------------|--|-----|
| Rayon Elium® composite | 77.5 | 2 | 3.2 | 0.2 | 10.2 | 1 |
| Jute Elium® composite [20] | 46.7 | 3 | 7.9 | 0.5 | 4.7 | 0.4 |
| Ramie Elium® composite [21] | 66 | 3 | 9.8 | 0.8 | 6.6 | 1.3 |

ANOVA analysis for the tensile strength of the above-mentioned composites is displayed in Table 2, which includes the variance of the tensile strength i.e. between groups (BG) and within group (WG). SS refers to the sum of square and df stands for degree of freedom. The F is the ratio of the BG mean square (MS) to the WG mean square. For all three composites, 5 samples were considered, therefore there were 15 counts in total. If the P-value of the F-test is less than 0.05, as reported here, the difference between the average tensile strength from one type of composite to another at 95% confidence level is statistically significant. Table 3 shows the ANOVA analysis of the tensile modulus; similarly, the P-value was calculated less than 0.05, indicating a statistically significant difference between the average tensile modulus from one composite to another at the confidence level of 95%.

Table 2. ANOVA analysis for the tensile strength.

| Source of Variation | SS | df | MS | F | P-value |
|---------------------|---------|----|---------|--------|---------|
| Between Groups | 2429.33 | 2 | 1214.66 | 140.29 | ~0 |
| Within Groups | 103.89 | 12 | 8.65 | | |

Table 3. ANOVA analysis for the tensile strength.

| Source of Variation | SS | df | MS | F | P-value |
|---------------------|--------|----|-------|--------|---------|
| Between Groups | 121.52 | 2 | 60.76 | 237.41 | ~0 |
| Within Groups | 3.071 | 12 | 0.25 | | |

It was detected that the rayon fiber treatments with acetylation, 3-methacryloxypropyltrimethoxy silane (MPS) and 3-aminopropyltriethoxy silane (APS) were found to reduce the tensile strength by 2.1%-35% and modulus by 2%-24% of the resulting composites; however, the elongation slightly increased only for MPS treated rayon fiber unsaturated polyester composite, as performed by one of the authors before [23]. The transfer of stresses from matrix to fiber, thus fiber-matrix interface is very important, which was not

achieved in these investigations. As the tensile properties are more fiber dependent, this explains the ineffectiveness of rayon fiber chemical modifications.

3.2. Scanning electron microscope (SEM) study of the tensile test

As illustrated in Figure 1, no indication of fabric delamination was detected in the cross-sectional image and the mode of fracture was fiber breakage. The sites of fractures are shown in Figure 1 (a) and fibers broke along the tension direction are displayed in Figure 1 (b). Good interfacial adhesion was observed between the rayon fibers and the Elium® matrix.

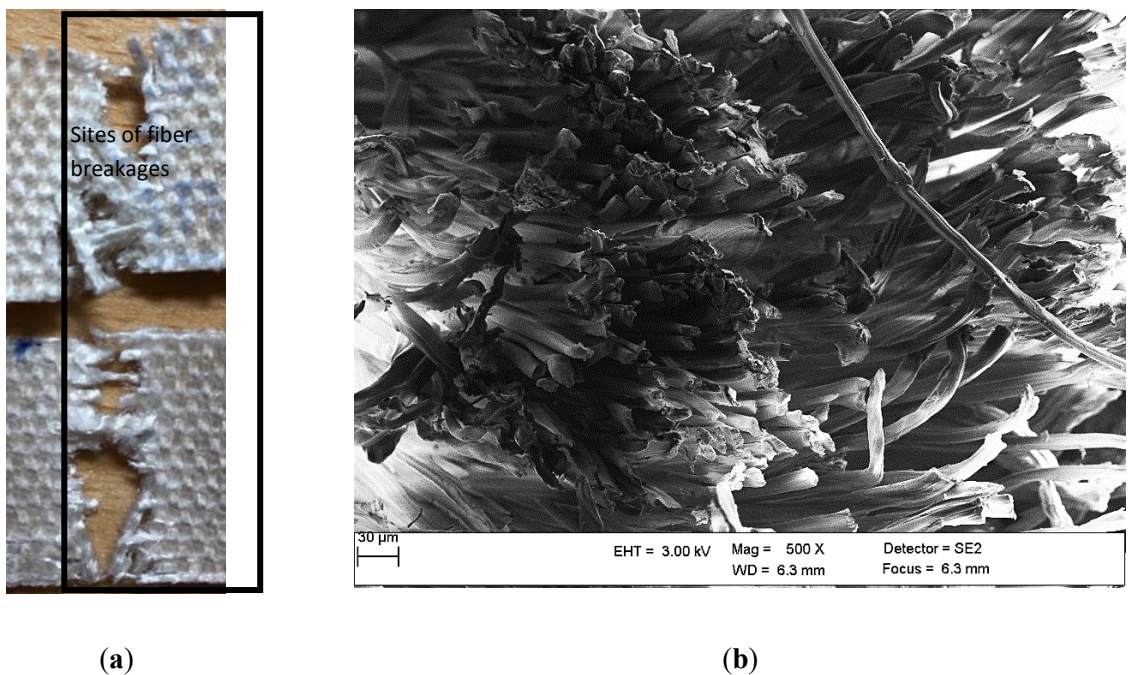


Figure 1. (a) Digital image and (b) cross-sectional SEM micrographs of fracture rayon composite sample after tension at 500 X magnification.

3.3. Flexural test analysis

The three-point bending strength and modulus of rayon fibre reinforced Elium® composite samples were measured in order to evaluate the properties and compare them with those of natural (ramie and jute) fibre Elium® composite systems as well as rayon fibre epoxy composites, fabricated via the same production method. The stress-strain curves of rayon fibre reinforced Elium® composite samples are displayed in

Figure 2 and the average flexural strength and modulus are tabulated (Table 4). The values are 93.5 MPa and 5.6 GPa for strength and modulus, respectively, which are in the same range of rayon fiber epoxy composite (as described in the previous work) [24]. 0°/90° woven jute fabric Elium® was found to show lower strength (7%) and modulus [20].

It was shown that chemical treatment of rayon fibers did not lead to the enhancement of flexural properties of their respective composites. For instance, γ -aminopropyltriethoxysilane (APTES) was used to modify the rayon fiber surface and in some composites, silane-coupling agent was used for incorporation into the epoxy system; however, no improvement was recorded for the flexural performance of the developed rayon epoxy composites [24]. In another investigation of the author [23], 3-methacryloxypropyltrimethoxy silane (MPS) and acetic anhydride were employed for silane and acetylation treatments of the rayon surface to produce treated rayon unsaturated polyester composites, which did not provide positive results for bending modulus and strength.

It was observed that the bending samples did not fracture even after 7 % bending strain; instead, very tiny cracks were observed on the tensile and compressive sides of the samples. On the tension and compression surfaces of the bent samples, the matrix became whiter and less transparent due to the breakage of polymer chains (Figure 3 (a) and (b)). The cross-sectional views of the bent samples were detected to illustrate no signs of delamination or breakage, as depicted in Figure 3 (c).

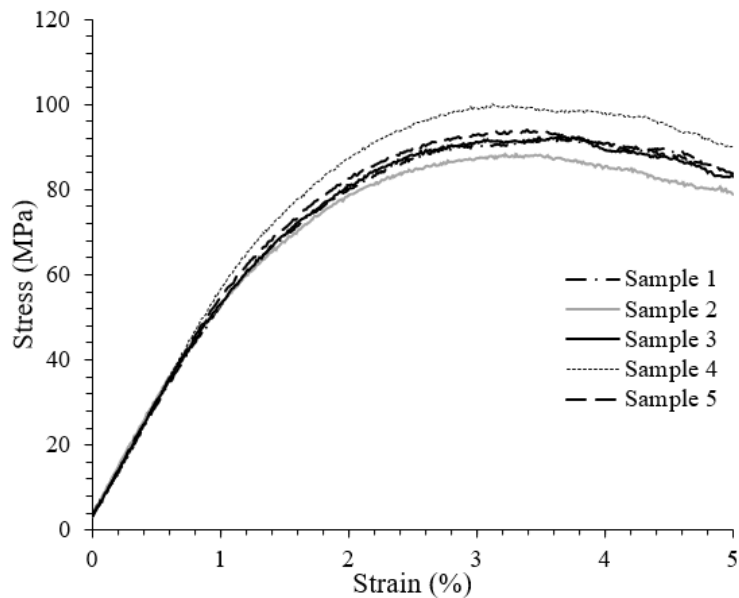


Figure 2. Stress-strain behavior of rayon composite samples.

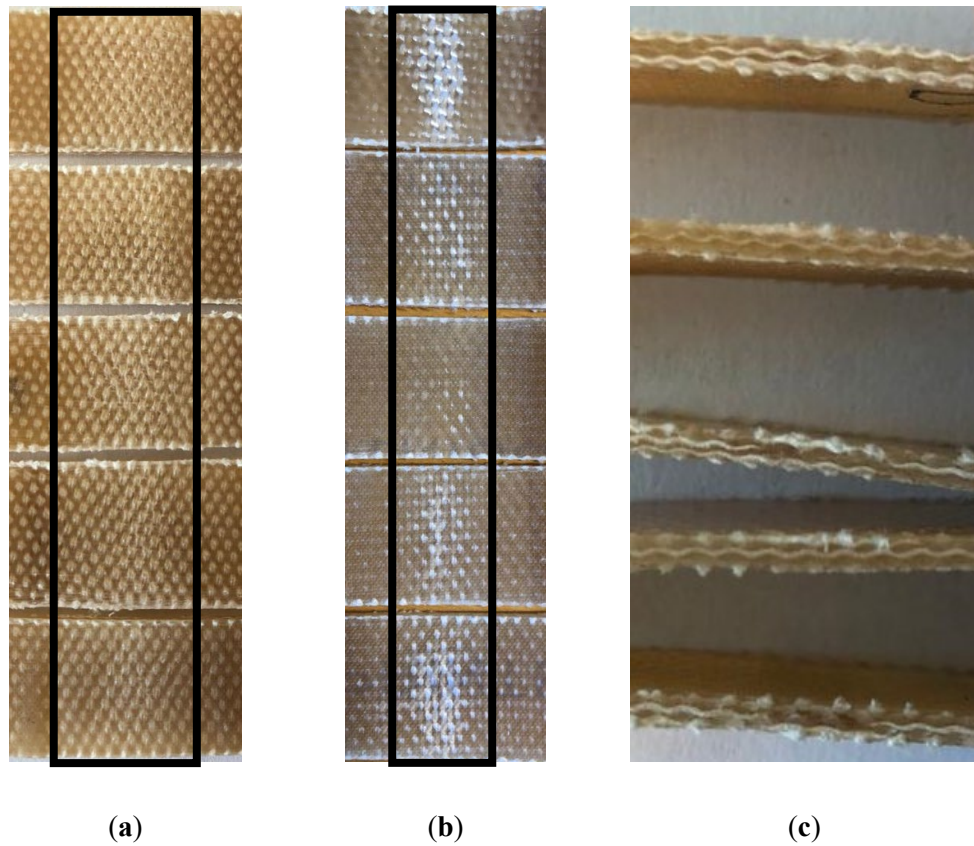


Figure 3. Digital images of (a) the middle of samples' bottom surfaces undergone tension, (b) the middle of samples' top surfaces undergone compression and (c) cross-sectional view of the bent samples right in the middle after flexural tests.

Table 4. Comparative average flexural strength and modulus of rayon fiber composite.

| Composites | Flexural strength (MPa) | STD (MPa) | Flexural modulus (GPa) | STD (GPa) |
|----------------------------|-------------------------|-----------|------------------------|-----------|
| Rayon Elium® Composite | 93.5 | 3.8 | 5.6 | 0.4 |
| Rayon epoxy composite [24] | 93.7 | ~3.7 | - | - |
| Jute Elium® composite [20] | 87.1 | 4.4 | 4.2 | ~0.1 |

ANOVA analysis tabulated (Table 5 and Table 6) shows the variance of flexural properties for the rayon Elium® composite and jute Elium® composite. The variance of flexural strength calculated between the groups and within groups (each group contains the result of 5 samples) demonstrated that the P-value equals 0.05. This implies that the difference between the flexural strength of these two composites was relatively significant at slightly less than 95% confidence level. This value could be explained by the fact that bending test is more matrix dependent and as the same matrix was used to make these two composites, the results can partly overlap. However, the P-value was obtained less than 0.05 from the F-test of the modulus values, which indicates a statistically significant difference between the average flexural modulus of these two composites at the confidence level of 95%.

Table 5. ANOVA analysis for the flexural strength.

| Source of Variation | SS | df | MS | F | P-value |
|----------------------------|-----------|-----------|-----------|----------|----------------|
| Between Groups | 101.41 | 1 | 101.41 | 5.29 | 0.05 |
| Within Groups | 153.33 | 8 | 19.16 | | |

Table 6. ANOVA analysis for the flexural modulus.

| Source of Variation | SS | df | MS | F | P-value |
|----------------------------|-----------|-----------|-----------|----------|----------------|
| Between Groups | 4.06 | 1 | 4.06 | 34.46 | 0.00037 |
| Within Groups | 0.94 | 8 | 0.11 | | |

3.4. Flexural test simulation and prediction of bending behaviour of a car door panel

Besides, in order to have a better understanding of the performance of the bio-based composite in an actual part, first finite element (FE) simulation of the bending scenario was calibrated and validated with the experiment, and subsequently, the materials model was applied to a car door panel for predicting the behavior of the component under flexural loading.

The whole flexural setup was designed according to the experiment, as shown Figure 4, and materials model was adopted as per the experiment test result. The width, length and span of the sample were 20 mm, 80 mm and 64 mm, respectively, and it was modelled as a homogeneous shell. The supports and the load which are presented as cylinder, measuring the diameter of 5 mm, were modelled as rigid. The modulus was obtained from the experiment and density and Poisson's ratio were 1.29 g/cm³ and 0.37 [25,26], respectively. Coulomb friction was used to model the friction between surfaces with a coefficient equal to 0.2 [27]. The polynomial materials modelling was assumed to model the plastic constitutive behavior. The bottom cylinders were fixed in all directions and rotations whereas the top cylinder was fixed in the x and z directions and can only move downwards (along the y direction). The mesh type of the sample was a 2D shell quad with the element size of 1 mm and the number of elements was counted 1440. The parameters above were found optimal in terms of computational time and accuracy convergence after performing some preliminary investigations of the element size. The FE model with the mesh and the color representation of the von mises stress subjected to the bending load is displayed in Figure 4 (a) and (b), and a vertical displacement of 18 mm was registered in the center of the sample.

A polynomial function of degree two was used to estimate the plastic deformation of the sample and is obtained as

$$\sigma = \sum_{k=0}^n a_k x^k, \quad (1)$$

Where σ is the stress (in MPa), x is the instantaneous strain, a_k is the strain amplitude and k is the strain exponent. Polynomial expression fitted the experimental results by using the strain amplitudes of a_2 , a_1 and a_0 which employed as approximately 8, 54 and 10, respectively, and the strain exponent of $k=2$. All these parameters were extracted with a coefficient of determination (R²) of 99%.

A comparison between FE model results in terms of force-displacement and the experimental measurements is depicted in Figure 5. Generally, a good agreement was obtained between the experimental result and the FE simulation. The small deviation in the plastic region is due to the fact that the average Poisson's ratio used for this simulation was the value obtained from the literature, which could not demonstrate the precise amount. This validated the developed model and enabled its utilization for the prediction of the bending performance of the real-life component.

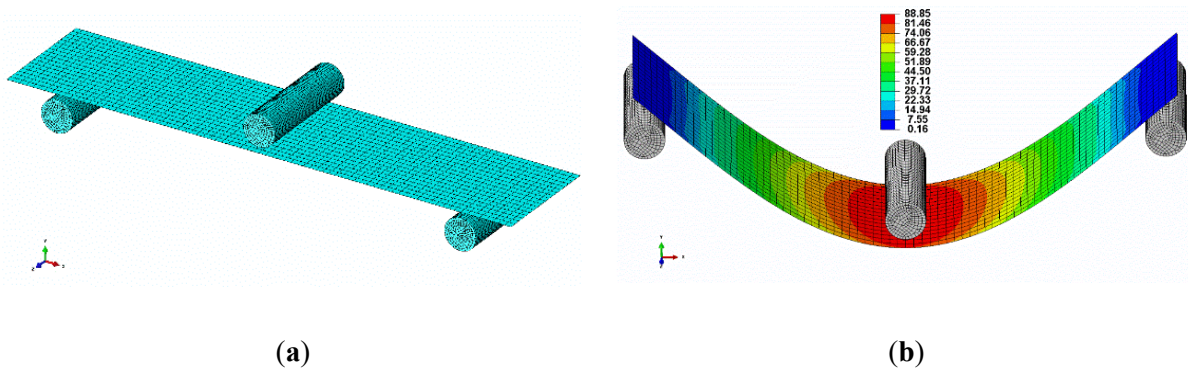


Figure 4. (a) FE model perspective of the bio-based composite sample and (b) the von mises stress applied to the specimen.

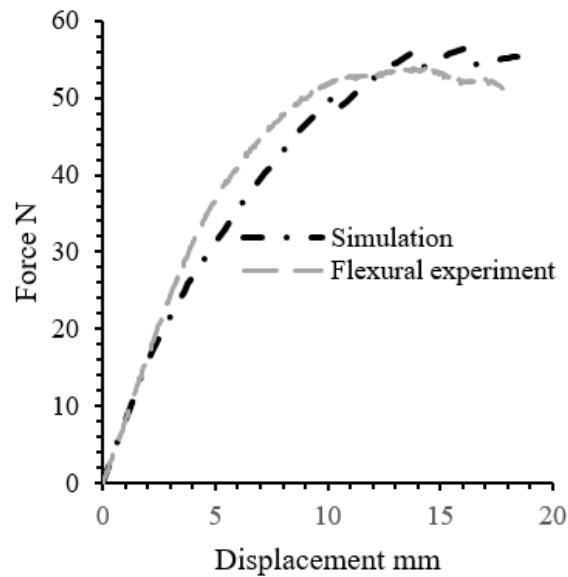


Figure 5. Force-displacement simulation of three-point bending scenario.

The simulation enabled to assess the displacement-force performance and deformation of the car door panel made of the same developed material in a bending scenario.

The swift car door panel [28] was used to simulate the bending of the part, which was modelled with the same materials model used for the bending test validation, under the flexural load in the shape of a sphere measuring 100 mm diameter. The friction coefficient of 0.2 was applied for the interaction between surfaces. The sphere placed in such a way to bend the middle of the door panel and its position from the bottom right corner of the door panel was 337 mm and 284 mm in the x and z directions, respectively. The

dimension and mesh of the door interior are depicted in Figure 6. The FE model of the whole assembly i.e. the sphere and the door panel is also shown in Figure 7. All the parameters were adjusted in accordance with the materials model developed in the flexural test experiment. The door panel was fixed from all the edges and the displacement to the -Y direction was enabled in the assembly. When the sphere went down into the middle of the component, the maximum load was obtained at the deflection of around 100 mm (Figure 8 (b)). However, the deflection could be much lower if the panel was supported by the door exterior. It is worth mentioning that the von mises stress obtained (~ 86 MPa) was close to that of the bending test scenario (Figure 8 (a)). Eventually, the prediction of the deflection-force behavior of the car door panel bent by the ball is shown in Figure 9. At around 102 mm deflection, a maximum load of approximately 20 kN could be recorded. This sort of materials modelling and structural simulation could contribute to the prediction of the performance and deformation of the automotive interior components, which can be fabricated using bio-based composites.

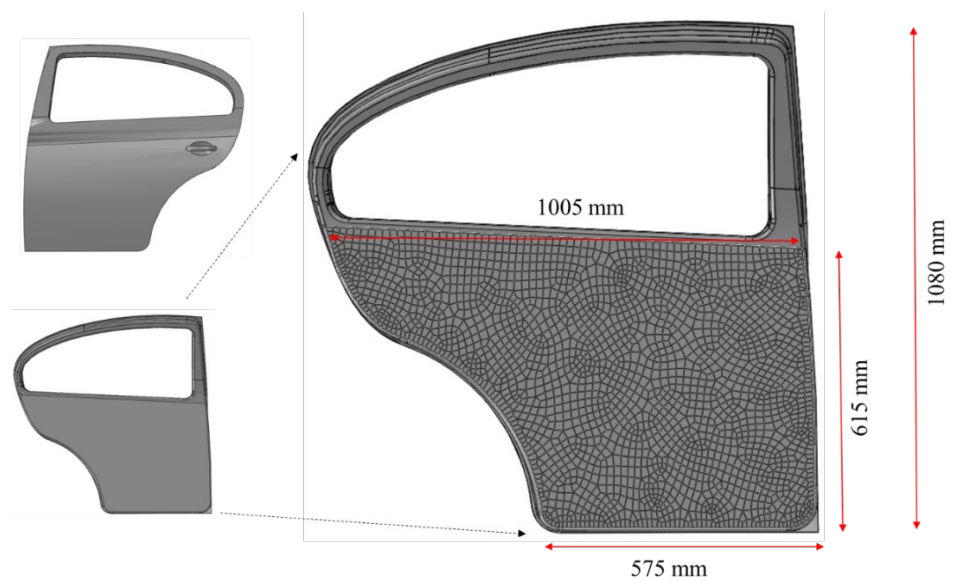


Figure 6. The mesh and dimension of the car door interior.

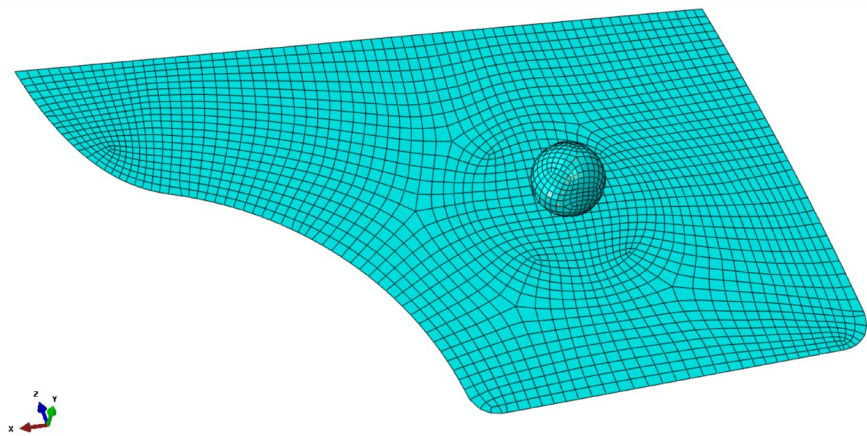


Figure 7. FE model perspective of the panel and the sphere.

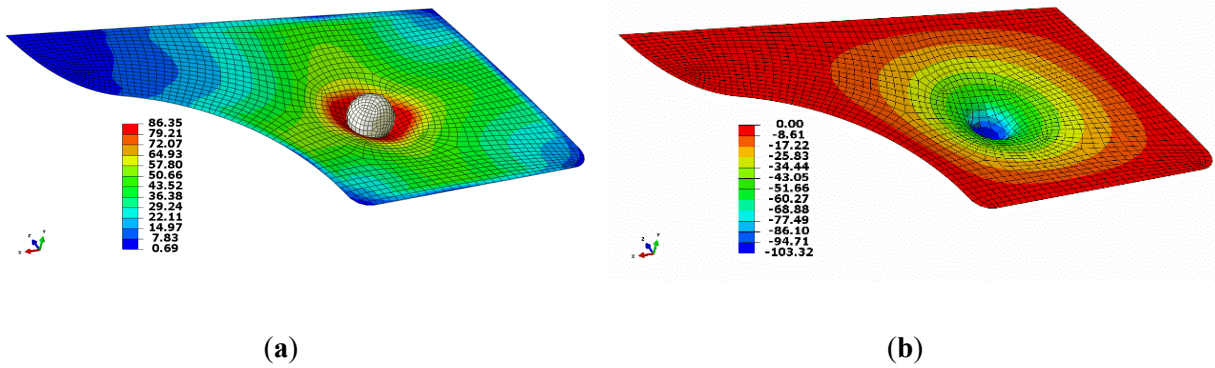


Figure 8. Deformed shape of the door interior: The color representation of (a) von mises stress and (b) vertical displacement.

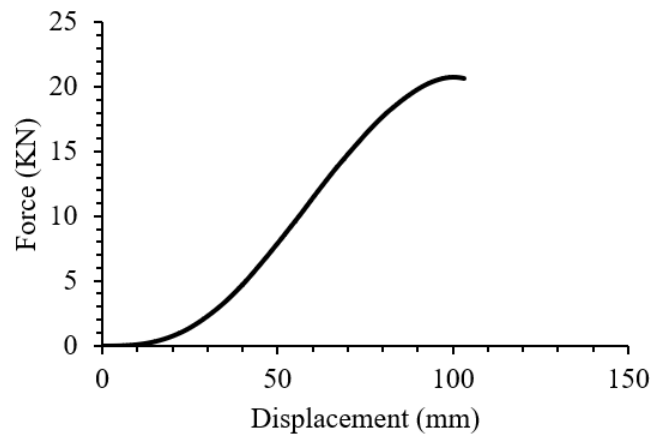


Figure 9. Prediction of the force-displacement behavior of the car door panel made of regenerated cellulose fabric Elium® composite.

DMA test was also performed to investigate the viscoelastic properties of rayon fiber Elium composite and to compare them with those of NF polymeric composites investigated by the authors, as shown in Figure 10.

The storage modulus (E') was measured 5.8 GPa at 30 °C which is in good agreement with flexural modulus as obtained from three-point bending test at room temperature. The glassy state region lasted until 80 °C where glass transition phase initiated, as illustrated in E' curve. The glass transition zone continued until about 100 °C with a swift continuous drop in E' .

It can be found out that the glass transition temperature of rayon fiber reinforced Elium® composite (107.7 °C), as obtained from the loss factor peak ($\tan(d)$), is higher or comparable with that of rayon epoxy systems and other natural fiber Elium® counterparts. The standard deviation of the T_g value for the composite is shown in parentheses in Table 7.

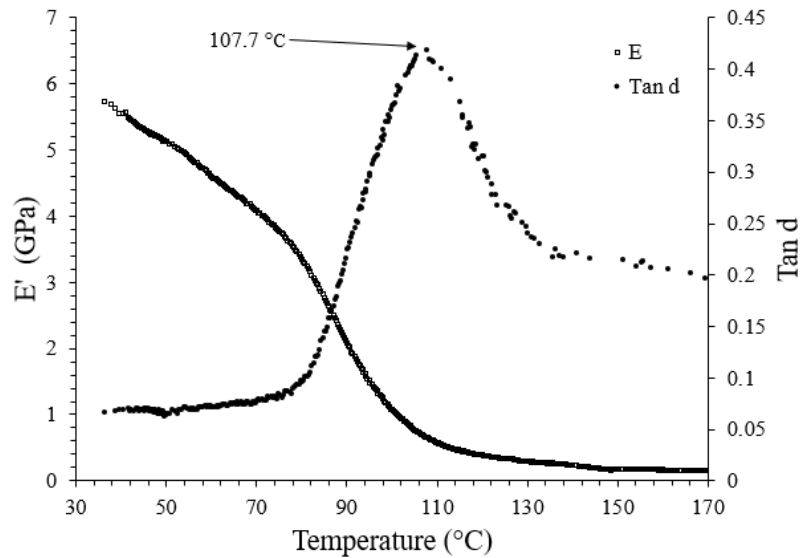


Figure 10. Average T_g as obtained from DMA analysis.

Table 7. Comparative T_g values of Elium® and epoxy composite systems with rayon and NF reinforcements.

| Composite samples | T_g |
|-------------------|-------|
|-------------------|-------|

| | |
|-----------------------------|---------------------|
| Rayon Elium® Composite | 107.7 (± 0.2) |
| Rayon epoxy Composite [24] | ~95 |
| Raime Elium® Composite [21] | 99 |
| Jute Elium® Composite [20] | 108.1 |

The whole mechanical results and viscoelastic analysis demonstrate the great potential of the developed bio-based composite for the interior applications, and structural simulation can be performed to initially predict the mode of deformation and expected force in the component.

4. Conclusions

A series of experimental tests were conducted to evaluate the mechanical properties of a viscose-type fabric reinforced thermoplastic composite. It was indicated that the developed material has good potential to be used for interior applications, which was one of the main aims of this study. In terms of strength, elongation and flexural properties, the regenerated cellulose fabric thermoplastic bio-composite demonstrated superior performance (or comparable) than those of NF epoxy or Elium® composite ones whereas the Young's modulus was found to be lower. It was indicated by one-way ANOVA analysis that the difference between the rayon Elium® composite and the other counterparts for the tensile and flexural properties was statistically significant; however only for the flexural strength the confidence level was slightly less than 95%. T_g was recorded a suitable value of 107.7 °C, placing the developed bio-composite at a comparable level. Moreover, the polynomial material model was fitted and predicted the plastic deformation and forces subjected to the sample under the bending load in the ABAQUS software. The materials FE model was applied to a car door panel which was bent by a sphere measuring 100 mm diameter, and the deformation-force behavior of the part was predicted.

The regenerated cellulose fabric thermoplastic composites reveal great potential for semi structural applications, and this can be evaluated together with materials simulation before making the whole part or testing the bio-composite component.

Funding: This research was funded by ÅForsk foundation, grant number 20-412.

Acknowledgments: Special thanks to Arkema for sponsoring the thermoplastic resin and to Cordenka for sponsoring the rayon fabrics.

References

1. Ganster, J.; Fink, H.-P.; Pinnow, M.J.C.P.A.A.S.; Manufacturing. High-tenacity man-made cellulose fibre reinforced thermoplastics–injection moulding compounds with polypropylene and alternative matrices. **2006**, *37*, 1796-1804.
2. Khalili, P.; Kádár, R.; Skrifvars, M.; Blinzler, B. Impregnation behaviour of regenerated cellulose fabric Elium® composite: Experiment, simulation and analytical solution. *Journal of Materials Research and Technology* **2021**, *10*, 66-73, doi:<https://doi.org/10.1016/j.jmrt.2020.12.024>.
3. Ganster, J.; Fink, H.-P. Novel cellulose fibre reinforced thermoplastic materials. *Cellulose* **2006**, *13*, 271-280.
4. Bledzki, A.K.; Gassan, J. Composites reinforced with cellulose based fibres. *Progress in Polymer Science* **1999**, *24*, 221-274, doi:[http://dx.doi.org/10.1016/S0079-6700\(98\)00018-5](http://dx.doi.org/10.1016/S0079-6700(98)00018-5).
5. Shibata, M.; Oyamada, S.; Kobayashi, S.i.; Yaginuma, D. Mechanical properties and biodegradability of green composites based on biodegradable polyesters and lyocell fabric. *Journal of Applied Polymer Science* **2004**, *92*, 3857-3863.
6. Skrifvars, M.; Dhakal, H.; Zhang, Z.; Gentilcore, J.; Åkesson, D. Study on the mechanical properties of unsaturated polyester sandwich biocomposites composed of uniaxial warp-knitted and non-woven viscose fabrics. *Composites Part A: Applied Science and Manufacturing* **2019**, *121*, 196-206, doi:<https://doi.org/10.1016/j.compositesa.2019.03.025>.
7. Ganster, J.; Erdmann, J.; Fink, H.-P.J.P. Biobased composites. **2013**, *58*, 423-434.
8. Weigel, P.; Ganster, J.; Fink, H.-P.; Gassan, J.; Uihlein, K. Polypropylene-cellulose compounds-High strength cellulose fibres strengthen injection moulded parts. *Kunststoffe-Plast Europe* **2002**, *92*, 95-95.
9. Fink, H.P.; Ganster, J. Novel Thermoplastic Composites from Commodity Polymers and Man-Made Cellulose Fibers. In Proceedings of the Macromolecular Symposia, 2006; pp. 107-118.
10. Khalili, P.; Tshai, K.; Kong, I. Natural fiber reinforced expandable graphite filled composites: Evaluation of the flame retardancy, thermal and mechanical performances. *Composites Part A: Applied Science and Manufacturing* **2017**, *100*, 194-205.
11. Offringa, A.R.J.C.P.A.A.S.; Manufacturing. Thermoplastic composites—rapid processing applications. **1996**, *27*, 329-336.

12. Chou, P.J.; Ding, D.; Chen, W.-H.J.J.o.r.p.; composites. Damping of moisture-absorbed composite rackets. **2000**, *19*, 848-862.
13. Sadighi, M.; Rabizadeh, E.; Kermansaravi, F.J.J.o.m.p.t. Effects of laminate sequencing on thermoforming of thermoplastic matrix composites. **2008**, *201*, 725-730.
14. Dordevic, D.; Necasova, L.; Antonic, B.; Jancikova, S.; Tremlová, B. Plastic Cutlery Alternative: Case Study with Biodegradable Spoons. *Foods* **2021**, *10*, 1612.
15. Van Rijswijk, K.v.; Bersee, H. Reactive processing of textile fiber-reinforced thermoplastic composites—An overview. *Composites Part A: Applied Science and Manufacturing* **2007**, *38*, 666-681.
16. Bhudolia, S.K.; Perrotey, P.; Joshi, S.C. Optimizing Polymer Infusion Process for Thin Ply Textile Composites with Novel Matrix System. **2017**, *10*, 293.
17. Khalili, P.; Blinzler, B.; Kádár, R.; Blomqvist, P.; Sandinge, A.; Bisschop, R.; Liu, X. Ramie fabric Elium® composites with flame retardant coating: Flammability, smoke, viscoelastic and mechanical properties. *Composites Part A: Applied Science and Manufacturing* **2020**, *137*, 105986, doi:<https://doi.org/10.1016/j.compositesa.2020.105986>.
18. Pisanu, L.; Santiago, L.C.; Barbosa, J.D.V.; Beal, V.E.; Nascimento, M.L.F. Effect of the process parameters on the adhesive strength of dissimilar polymers obtained by multicomponent injection molding. *Polymers* **2021**, *13*, 1039.
19. Fajardo Cabrera de Lima, L.d.P.; Santana, R.M.C.; Chamorro Rodríguez, C.D. Influence of coupling agent in mechanical, physical and thermal properties of polypropylene/bamboo fiber composites: under natural outdoor aging. *Polymers* **2020**, *12*, 929.
20. Khalili, P.; Blinzler, B.; Kádár, R.; Bisschop, R.; Försth, M.; Blomqvist, P.J.M. Flammability, Smoke, Mechanical Behaviours and Morphology of Flame Retarded Natural Fibre/Elium® Composite. *Materials* **2019**, *12*, 2648.
21. Khalili, P.; Blinzler, B.; Kádár, R.; Blomqvist, P.; Sandinge, A.; Bisschop, R.; Liu, X. Ramie Fabric Elium® Composites with Flame Retardant Coating: Flammability, Smoke, Viscoelastic and Mechanical Properties. *Composites Part A: Applied Science and Manufacturing* **2020**, *137*.
22. Adusumali, R.B.; Reifferscheid, M.; Weber, H.; Roeder, T.; Sixta, H.; Gindl, W. Mechanical properties of regenerated cellulose fibres for composites. In Proceedings of the Macromolecular symposia, 2006; pp. 119-125.

23. Rajan, R.; Riihivuori, J.; Rainosalu, E.; Skrifvars, M.; Järvelä, P.J.J.o.R.P.; Composites. Effect of viscose fabric modification on the mechanical and water absorption properties of composites prepared through vacuum infusion. **2014**, *33*, 1416-1429.
24. Rajan, R.; Rainosalu, E.; Ramamoorthy, S.K.; Thomas, S.P.; Zavašnik, J.; Vuorinen, J.; Skrifvars, M.J.J.o.A.P.S. Mechanical, thermal, and burning properties of viscose fabric composites: Influence of epoxy resin modification. **2018**, *135*, 46673.
25. Radzuan, N.A.M.; Tholibon, D.; Sulong, A.B.; Muhamad, N.; Che Haron, C.H. Effects of High-Temperature Exposure on the Mechanical Properties of Kenaf Composites. *Polymers* **2020**, *12*, 1643.
26. Fajrin, J.; Zhuge, Y.; Bullen, F.; Wang, H. Flexural behaviour of hybrid sandwich panel with natural fiber composites as the intermediate layer. *Journal of Mechanical Engineering and Sciences* **2016**, *10*, 1968-1983.
27. Abdolpour, H.; Garzón-Roca, J.; Escusa, G.; Sena-Cruz, J.M.; Barros, J.A.; Valente, I.B. Development of a composite prototype with GFRP profiles and sandwich panels used as a floor module of an emergency house. *Composite Structures* **2016**, *153*, 81-95.
28. Available online: <https://grabcad.com/library/swift-car-door-shape-design-1>.

Chapter 3




Journal of Materials Research and Technology

Volume 22, January–February 2023, Pages 3423-3435



Original Article

Regenerated cellulose fabric reinforced bio-based polypropylene sandwich composites: fabrication, mechanical performance and analytical modelling

Pooria Khalili ^a  , Mikael Skrifvars ^a, Hom Nath Dhakal ^b, Chulin Jiang ^b

^a Faculty of Textiles, Engineering and Business (Swedish Centre for Resource Recovery), University of Borås, 510 90, Borås, Sweden

^b Advanced Polymers and Composites (APC), School of Mechanical Design and Engineering, University of Portsmouth, PO1 3DJ, Portsmouth, UK

Regenerated Cellulose based fabric thermoplastic composites: Fabrication, mechanical performance, and simulation

SUMMARY

Sandwich composites were fabricated successfully with the balsa wood as core material and regenerated cellulose fabric bio-based polypropylene (PP) composite skins. The regenerated cellulose fabric PP composites were produced using two different methods: the conventional stacking lay-up and directly using PP pellets. Sandwich composites were made using the hot press equipment with the customized mold. The sandwich composite system and bio-composite laminate were designed to achieve very close weight to compare the key mechanical properties that each design can bear. It was evidenced from the experimental results that 416% increase in the bending load bearing property of the part can be obtained when sandwich structure was used. These experimental results were in close agreement with one of the analytical modelling utilised. The drop weight impact test results demonstrated that the sandwich specimen is capable of withstanding more than 6 kN load and absorbing the impact energy of 28.37 J.

1. Introduction

Man-made regenerated fibers have been demonstrated to provide substantial promise as reinforcing agents in thermoplastic systems both in the form of short fibers [1, 2] and continuous fibers [3]. They offer the merits of both natural and synthetic fibers, which comprise on the one hand low density, CO₂ neutrality, non-abrasiveness to manufacturing equipment and biodegradability of natural fibers (NFs) [4-7], and on the other hand, physical, mechanical and uniform morphological properties of synthetic fibers. Diverse manufacturing routes together with different matrices were experimented to produce rayon (man-made regenerated fiber) thermoplastic systems spanning melt mixing processing followed by injection molding [2, 8-10], resin infusion method [3, 11] and compression molding for long fiber material systems.

Polypropylene (PP) is a commonly used matrix on account of lowest price and density in comparison with other polymer materials [12] and even other bio-polymers such as polylactic acid (PLA). Glass fibers (GF) are used as a reinforcement in many applications, however, recent research has been paid special attention to the substitution of GF with NF reinforced PP composites, which possess lower density compared to GF/PP counterparts [12]. These characteristics meet, in particular, the requirements of transport industries where vehicles should be low in weight to decrease fuel consumption and are made of potentially low cost and sturdy materials [13]. Over the last years, the necessity for broadening crude materials and the environmental awareness pursue attempts at use of recourses with renewable nature. Regenerated cellulose fibers offer these merits while inducing good performance. Low density and high

tenacity provide high specific strength of resulting PP composites which fit the requirements of lightweight applications. These bio-based composites can be incinerated after utilization [8, 10].

The structural properties of regenerated cellulose fabric PP composites can be tailored to reach the desired requirements. For semi-structural applications, sandwich composites are one of the main structures or forms of panels used in industry [14]. Sandwich structures provide low weight and high mechanical properties. Presently, these types of structures are utilised in packaging, automotive, construction and aviation industries among others [15]. These panels consist of two facings bonded to a thick, lightweight core material. Composites and metals are principally used as facings whereas honeycomb structures, foams and balsa wood are the choices of the core material [16]. Employment of NFs in panels is a new research area, and hitherto limited investigations have been performed [17]. Kolahchi et al. [18] studied the buckling of polymeric composite structure containing carbon nanotube (CNT) and carbon fiber for aircraft conical shells and modeled it based on Halpin-Tsai theory, stability performance [19] of magnetostrictive facings loaded with graphene platelets as well as the vibration properties and Young's modulus of polymeric composites consisted of graphene platelets and piezoelectric layers [20].

Different theories can be used to predict the properties of composites: e.g. Mori-Tanaka model was used as the basis to study the effect of earthquake load on concrete pipes reinforced by fiber reinforced composites [21]. In another investigation [22], a method on the basis of Hamilton was selected to obtain the dynamic behaviours of sandwich nanocomposite conical shell in magnetic and thermal conditions. Al-Furjan et al. [23] studied the effective properties of nanocomposite using Halpin-Tsai micromechanics model. The material system was a micro sandwich beam containing core of elastomer.

Replacement of GF with NFs in the sandwich panels was found to enhance the vibration damping and sound properties [24] and to promote significant environmental merits [25] of structures containing thermoset polymers. In another study, synthetic PP polymer and jute fabrics were hot pressed to produce sandwich composites with polyethylene terephthalate (PET) foam, honeycomb PP and balsa core materials [17]. It was found out that the flexural rigidity increased outstandingly as compared to that of composites without the core. It was also revealed that laminates with the balsa wood core demonstrate greater bending rigidity than the panels with other cores used in this investigation. Some models are used to predict the mechanical performance of the composite structures. For instance, sandwich composites filled with graphene platelets were modelled based on the Halpin-Tsai micromechanics theory to obtain Young's modulus [26]. Several methods of tensile test studies for fiber reinforced polymeric composites were reported in Al-Furjan et al. article [27].

Very few works have been reported on utilization of regenerated cellulose fabrics in sandwich panels. Moreover, to the best of authors' knowledge, utilization of bio-based PP in sustainable sandwich bio-composites has not been investigated prior. The combination of the regenerated cellulose fabric (rayon in this study) and the bio-based PP were not considered for composite production as either composites or facing materials used in panels thus far. In this work, the above-mentioned composite laminate and bio-based sandwich composites were manufactured. The PP polymer used had about 30% bio content and labelled as recyclable like other synthetic PPs. It is specified as a grade of high impact resistance, good processability and medium stiffness. This PP grade is processed similar to other synthetic PP types in order to make parts. The effect of incorporation of rayon fabrics in the bio-based PP in terms of tensile and flexural properties was investigated. The impact of inclusion of the polymer in the forms of pellets and films on the mechanical properties of the composites were also studied. The bending behavior of sandwich bio-based composite, balsa wood and the control composite were focused, and the flexure of sandwich panel was modelled with Euler-Bernoulli and Timoshenko theories. Additionally, the load bearing capability and energy absorption performance of sandwich structure under low velocity impact test was also investigated, which were not focused much on previous experiments before with these constituents included in the composite skins.

2. Materials and methods

2.1. Materials

The bio-based PP containing around 30 % bio-based content was purchased from NaturePlast, France. PP possessed the density (23 °C) and melt flow index (230 °C) of 0.9 g/cm³ and 70 g/10min, respectively. 0/90 man-made cellulose (rayon) fabrics were provided by Cordenka company, Germany. The Cordenka® 700 2440 dtex had an areal weight and density of 442 g/m² and 2482 dtex, respectively. Balsa wood used as core material in the sandwich composite was purchased from hobbymodeller, Sweden, and had the density and thickness of 0.12 g/cm³ and 6 mm, respectively. Rayon fabrics were dried in a convection oven for a period of 24 h at 70 °C prior to the composite processing to avoid moisture absorption. PP films and pellets were also dried for the same time at 40 °C before further processing.

2.2. Film preparation and optimization

PP granules were compressed into films with the aid of a 20-ton manual bench press equipment (Rondol Technology Ltd., UK). The area, where granules was pressed, was measured 190 mm (length) × 190 mm (width) and it was aimed to obtain around 0.4 mm thick bio-based PP films. To achieve the target thickness,

varying compressive pressure and amounts of PP pellets were used for a period of 60 s at 200 °C. Ultimately, 0.8 bar pressure was applied to 10 g bio-based PP in order to attain the 0.4 mm thick film. This resulted in the target fiber mass fraction in the composite by optimizing the PP film thickness obtained by varying press pressure and PP quantity. Figure 1 illustrates the various process parameters used for optimisation of PP film thickness.

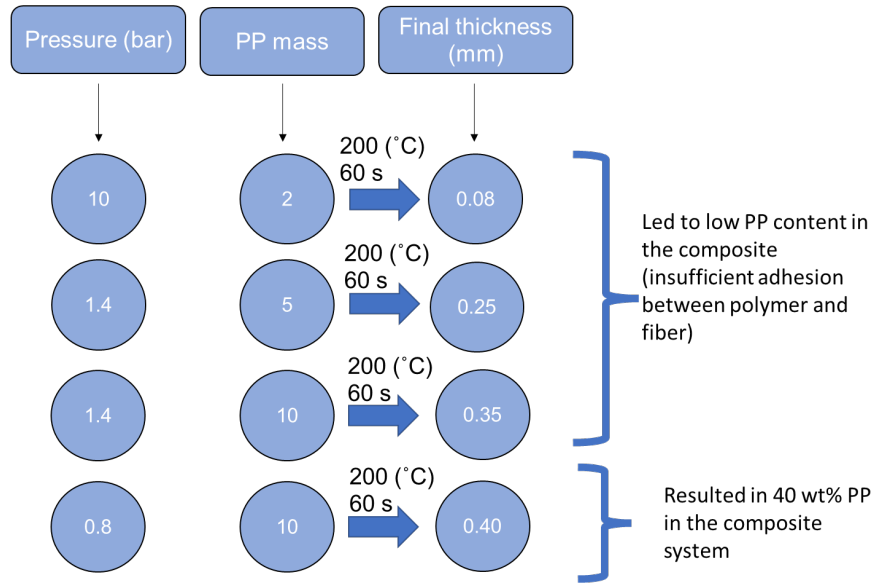


Figure 10. The method of optimization for PP film to obtain the required thickness.

2.3. Rayon PP composite and sandwich manufacturing

A conventional film-stacking method, constructed by the addition of alternating layers of man-made cellulose fabric and PP film, was used to produce rayon fabric PP-sheet composites using the same hydraulic hot press utilised for the film fabrication. After stacking the layers as per Figure 2 (which included three layers of rayon (R) and five sheets of PP film) in the 2 mm thick mold, the press pressure was gradually increased in 1 min to reach the level of 50 bar (5 MPa) at 200 °C. Then, the whole system was held for a period of 10 min for consolidation before cooling the material under 0.08 bar pressure for 180 min at room temperature (RT). The composite plates measuring 180 × 180 × 2 mm with the fiber mass fraction of 61.4 wt% was obtained from this manufacturing system.

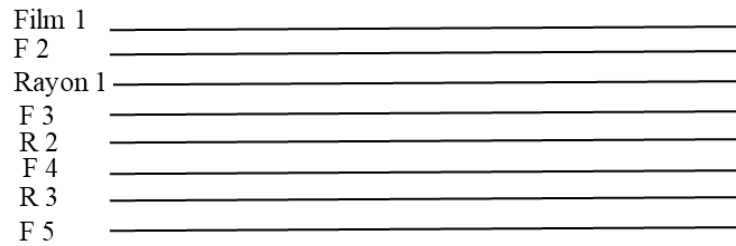


Figure 11. Composite laminate design.

A composite laminate production method with the aid of PP pellets was also performed for comparison purpose. PP pellets were manually distributed between the three layers of the rayon fabrics in the same 2 mm thick mold. The weight of fiber was subtracted from the mass of rayon reinforced PP film composite to use the same amount of PP for the composite fabricated with the direct use of PP pellets. The final mass of rayon reinforced PP pellet-based composite was then weighed to ensure that the same weight for both types of the composites was obtained. Exactly, the same fabrication conditions as described above were applied. The whole material system underwent continuous pressure in 1 min to reach 5 MPa pressure at 200 °C. The assembly was under the pressure for 10 min and subsequently, was cooled down with the same above-mentioned condition at the RT. In the same manner, neat bio-based PP polymer plate was also prepared with 100 wt% of the polymer as the control, measuring 2 mm thickness. It is worth mentioning that the wings and tails of a flying plane (toy), which was originally made from foam polymer, were successfully replaced with bio-based PP composites containing the balsa core as a demonstrator.



Figure 12. Flying wind demonstrator with the wings and tails made of bio-based sandwich composite with the balsa wood core.

The rayon bio-based PP sandwich composite with the balsa wood core was fabricated in such a way that a layer of rayon fabric was placed at the top and another one at the bottom of balsa wood. On top and bottom of each viscose fabric a layer of PP sheet was positioned and the whole assembly was placed in a mold measuring the cavity of $100 \times 100 \times 7$ mm (Figure 4). A layer of PTFE film was placed on the very top and bottom surface of the assembly for easy demolding. Ultimately, a bio-based sandwich composite with balsa as core material was produced and the resulting composite panel had the thickness of 7 mm. In order not to create permanent deformation to balsa wood while compacting, the whole sandwich composite was hot pressed for the same duration, 10 min, as rayon fabric PP sheet composite laminate was produced, at 0.5 MPa pressure (which was lower than the compressive strength of the balsa wood). The bending test samples were cut along the axial grain direction of the balsa wood using the laser cutting machine. Scanning electron microscope (SEM) tests were performed on the fractured bio-based panel and the balsa wood core.

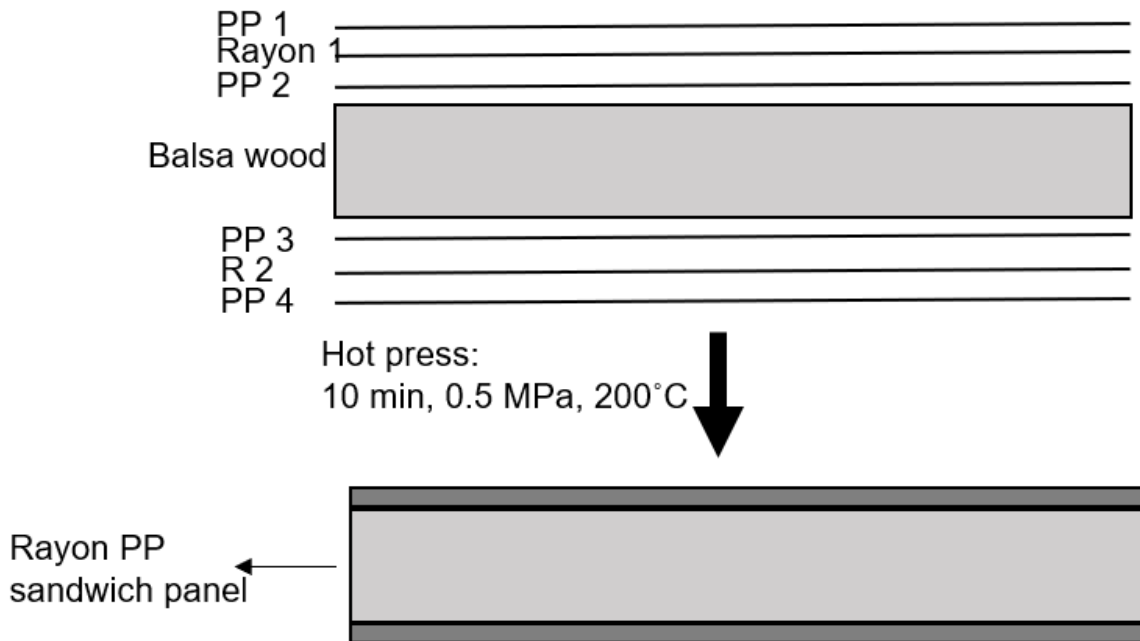


Figure 13. Schematic diagram of the sandwich composite preparation.

3. Characterizations

The neat PP, bio-based composite laminate and sandwich composite samples were tested under bending loading according to BS EN ISO 14125 [28] with the aid of a Tinius Olsen H10KT universal testing instrument and their flexural properties were compared. The crosshead speed of 5 mm/min, span length of 64 mm and sample dimension of 80 mm (length) \times 20 mm (width) were used for the tests. The load-cell of 250 N was connected to the equipment. All the specimens were conditioned for 24 h at the humidity of 50% and the temperature of 23 °C prior to the testing. The average values of the results were accordingly reported.

The tensile behaviors of dog-bone man-made cellulose fabric composite and neat PP polymer samples were investigated in accordance with EN ISO 527-4 (type 1B specimen) [29]. The crosshead speed of 2 mm/min, initial distance between the grips of 115 mm and span length of 50 mm was used for the tests. The equipment was connected to the load-cell of 5 kN and the instrument was equipped with a 100R mechanical extensometer. A GCC Laserpro Spirit GLS instrument was used for all the composite sample preparations. The samples were conditioned for 24 h at the temperature of 23 °C and the humidity of 50% prior to the testing.

The low velocity impact tests were performed on the sandwich composite and the balsa wood specimens using a Zwick/Roell HIT230F drop weight tester. Three sample dimensions measuring 70 \times 70 mm were cut by a laser cutting instrument (GCC Laserpro Spirit GLS, Borås, Sweden). The weight of impactor was 23.11 kg, which includes both impactor mass of 22.832 kg and tup mass of 0.278 kg. This creates a 25-joule incident energy by falling the impactor from the height of 110 mm at the ambient temperature. The diameter of the tup, which is made of the hemispherical steel, was 19.8 mm. The samples were mounted on the rigid clamping supports. With the aid of a strain-gauge striker and a load-cell installed on the machine several parameters were obtained. Displacement, force, time and absorbed energy were recorded during the tests. In order to prevent multiple impacts on the samples, an anti-rebound device was connected to the instrument.

SEM test was performed on the fractured sandwich bio-composite and balsa wood samples after the impact test to obtain the SEM micrographs. A Philips XL30CP SEM instrument was used to scan the impacted sandwich composites. The samples were first prepared by metallizing with a thin gold layer in a vacuum condition, and subsequently were scanned at a 15 kV voltage. The sandwich specimens after the bending and low velocity impact tests were found to have no debonding or delamination between the core and the

skins. Therefore, the specimen after the impact test was chosen, and the composite skin was scanned at the cross-section, where a separation between the fracture part and the whole specimen was formed, to investigate the microstructure of the composite skin after the fracture.

Digital imaging microscope tests were carried out to investigate the interfacial adhesion between the core and the composite skin in the sandwich panel and between the fabric layers and the bio-based PP polymer in the rayon PP sheet composite sample after the processing. An eclipse LV150N microscope- digital imaging combined with advanced optical system was used to capture the cross-sectional images of the samples without surface coating.

Differential Scanning Calorimetry (DSC) tests were performed on only the PPs selected from three different formulations, namely neat PP, rayon PP pellet and rayon PP film. This was to evaluate the crystallinity levels and melting behavior of the PP for these three formulations due to varying processing of PP in these material systems. A DSC-2000 apparatus (TA Instruments, USA) was used to test the samples. Samples weighing 5-10 mg were placed in covered aluminum crucibles. The samples were heated from -40 to 200 °C at a ramping rate of 10 °C/min in nitrogen atmosphere and the flow rate of nitrogen gas was set to 50 mL/min. Samples were maintained for 2 min at 200 °C to avoid the inclusion of the thermal history in the measurements. Then, the samples were cooled down to -40 °C at the same heating rate. The samples were kept for 2 min at -40 °C and subsequently were heated up to 200 °C at 10 °C/min heating rate. The measurements reported were from the second and third cycles of the tests.

4. Results

4.1. Bending properties of composites

The bending strength and modulus values of neat bio-based PP, man-made cellulose fabric PP sheet composites and man-made cellulose pellet composite laminates are displayed in Table 1. The bending strength and modulus were 22.8 MPa and 0.97 GPa for the control, respectively. The combination of rayon fabric and PP sheet to make the composite led to significant improvement in modulus (2.71 GPa) by 180 % increase. The strength was found to enhance by 13% as well. This demonstrates the reinforcing effect of bio-based fabrics in the composite. Using PP in the form of pellets in the composites was seen to enhance the flexural performance as compared to that of neat PP whereas the flexural strength and strain were found to decrease in comparison with those of rayon PP sheet composite laminate counterpart. This implies that PP sheets provide better distribution of PP in the fabric layers. Ganster et al. [8] investigated the bending properties of rayon tyre cord yarn reinforced PP composite for injection molding applications. The flexural

modulus was obtained approximately 2.60 GPa at the fiber weight fraction of ca. 40% in this study. Karaduman et al. [17] produced 15 wt% jute reinforced synthetic PP composite using the hot press equipment and the stiffness obtained was 1.88 GPa whereas the neat synthetic PP demonstrated the modulus of 1.20 GPa. These values prove the practicality of rayon bio-based PP composite systems with a high percentage of the bio content in terms of the mechanical behaviors.

The samples were examined after the tests, and it was found out that the neat PP and composite laminate samples did not break, and the mode of fracture was micro-cracks on their compression (top) sides. No sign of delimitation was also observed in the samples.

Table 2. Flexural properties of bio-based PP and rayon composites.

| Samples | Strength (MPa) | Strength SD (MPa) | Modulus (GPa) | Modulus SD (GPa) |
|-----------------|----------------|-------------------|---------------|------------------|
| Neat PP | 22.80 | 0.50 | 0.97 | 0.01 |
| Rayon PP sheet | 25.80 | 0.90 | 2.71 | 0.10 |
| Rayon PP pellet | 23.48 | 0.60 | 2.42 | 0.10 |

The intrinsic mechanisms of a sandwich panel are to provide a high stiffness (/weight ratio) as compared to material systems without core. A thicker core possessing less stiffness and strength than facings is bonded to two skins with stronger and stiffer properties. The material system promotes enhanced flexural performance with the incorporation of low density, thick and soft core whilst ensuring a panel of lightweight structure [14]. Sandwich composite samples with 6 mm thick balsa wood core were tested to compare with the rayon reinforced bio-based PP composite laminate specimens measuring 2 mm thickness. The sandwich composite was designed in such a way to have proximately the same weight as the composite laminate, as seen in the weight ratios in Table 2. The deflection-force curves of the sandwich composite, rayon PP laminate and balsa wood are shown in Figure 5. The bio-composite skin was found to offer approximately 21 N whereas the greatest force was recorded for the sandwich composite with the value of 107.3 N at the deflection of approximately 2.1 mm demonstrating 416 % increase in load-bearing potential of the part. This demonstrates the successful production and excellent effectiveness of the sandwich composites. Balsa wood was seen to reveal higher maximum force capacity (~46 N) than that of the composite laminate. It is

known that man-made cellulose fibers show lower stiffness than NFs [3, 30], and the incorporation of the core material can compensate significantly for this issue.

The force-displacement behaviors of all three types of materials were totally different and presented varying trends (Figure 5). The composite skin was seen to demonstrate an elastic-plastic deformation with a high value of elongation to break. Balsa wood tested along the grain direction was found to show greater stiffness than that of the bio-composite laminate along with a more kind of the elastic behavior. However, the sandwich bio-composite can be seen that proving a totally different behavior than the other two types of materials. The elastic slope of the sandwich composite was 14 times faster than that of the bio-based composite skin, which confirms again the great effectiveness of the sandwich composite for nearly the same weight as composite laminate. The sandwich composite provided a synergy in such a way that possesses enhanced properties in terms of force-displacement and ultimate load bearing capacity. Moreover, the displacement followed the trend of the bio-composite laminate i.e. a very long deflection.

Figure 6 illustrates the top and bottom surfaces of the balsa wood samples after the flexure. It can be observed that the material bent under the load and dented on the top surface (Figure 6 (a)). At the bottom of the specimens, a continuous crack along the width, right below where the load was applied, was observed. For the bio-based sandwich structures with the balsa wood core, the upper composite skin and the core, as shown in Figure 7 (a) and (b), were compressed and depicted a dent, respectively. The lower surface of the bio-based composite, however, experienced some micro cracks along the width of the specimens at the tension side of the panel (Figure 7 (c)). It is important to note that no sign of delamination was detected for the sandwich composites with the balsa core in this work, however, as investigated in another study, in case of PET foam and PP honeycomb based sandwiches with jute fabric composite skins, the panels experienced a significant delimitation under flexure [17]. Moreover, they stated that Balsa sandwich provided greater flexural performance than that of PET foam core and the PP honeycomb core sandwich bio-composites.

Table 3. Comparison between the bio-based composite skin and its respective sandwich structure, as obtained from the bending test results and flexural test specimens.

| Samples | Bio-composite skin | Sandwich composite along the wood grain direction | Balsa wood |
|----------------|--------------------|---|------------|
| Thickness (mm) | 2 | 6.8 | 6 |
| Weight (g) | 3.22 | 3.4 | 0.62 |
| Weight ratio | 1 | ~1.05 | - |

| | | | |
|---------------------|------|-------|------|
| Max. force | 20.8 | 107.3 | 45.8 |
| Initial slope ratio | 1 | 14 | 4.5 |

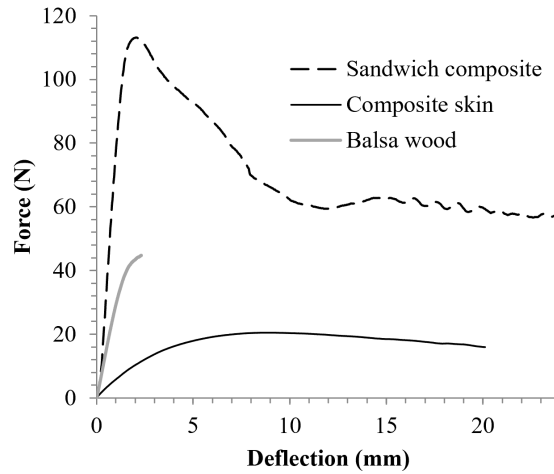


Figure 14. Comparison of force-deflection responses between sandwich composite, balsa wood and composite skin.



Figure 15. (a) The middle view of the top balsa wood samples and (b) the middle view of the bottom surface of the balsa wood samples after bending.

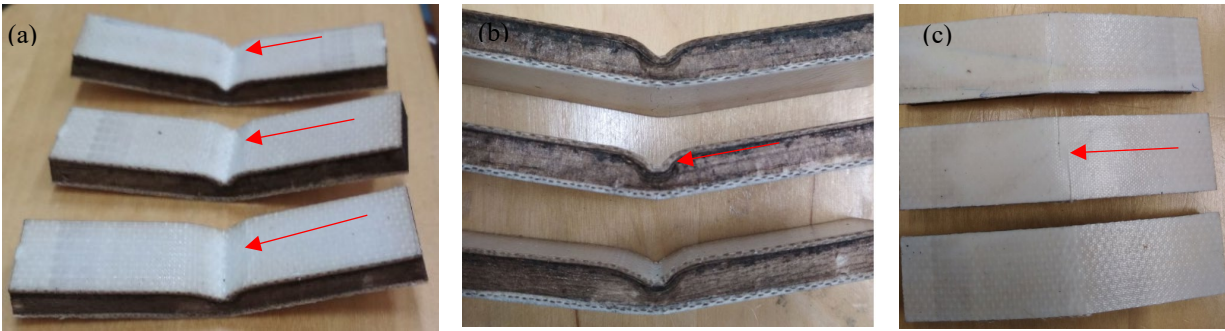


Figure 16. The images of the sandwich composites after the flexure: (a) the upper composite skin bent, (b) the core material bent together with the upper skin and (c) the bottom bio-based composite skin.

Modelling the bending properties of balsa wood sandwich bio-composites:

In order to predict the force-deflection behavior of sandwich composites the panel was modelled using both Euler-Bernoulli and Timoshenko beam theories, and the estimations of models were compared with the flexural test results. The boundary conditions were based on the two fixed supports with the span length of 64 mm where the sample was resting on and a load applied to the middle of the specimen allowing the displacement in -Y direction. According to Euler-Bernoulli beam theory, the differential equation of the displacement curve for beams loaded transversely is [31]:

$$EI \frac{d^2y}{dx^2} = -M \quad (1)$$

Where M is the flexural moment, I is defined as the moment of inertia of the cross-section (with regard to the neutral axis), and E is the elastic stiffness.

In the event of three-point bending force, the ultimate displacement (y_{max}) obtains in the middle of the beam as follows:

$$y_{max} = \frac{Pl^3}{48EI} \quad (2)$$

Where P is the bending force, l is the flexural span length, and EI is the bending rigidity, which, for the materials with core, can be obtained based on the equation below [32]:

$$EI = E_f \frac{btd^2}{2} \quad (3)$$

Where E_f is the tensile modulus of the skin, b is the width of the sandwich material, t is the thickness of each skin layer, and d is the distance between the central axes of the two facings.

The maximum displacement at the middle of the beam (y_{\max}) is obtained with the equation below:

$$y_{\max} = \frac{Pl^3}{24E_f btd^2} \quad (4)$$

The equation 4 (Euler-Bernouli) neglects the impact of shear, however Timoshenko model considers additional displacement as a result of shear forces. Therefore, the maximum displacement at the middle of the sandwich beam in three-point bending scenario is:

$$y_{\max} = \frac{Pl^3}{48EI} + \frac{\alpha Pl}{AG} \quad (5)$$

Where A is the cross-sectional area and calculated as $A = bd/c$ for sandwich composites (c is the core thickness), α is the shear correction factor and G is core shear modulus.

The two terms in equation 5 demonstrate the displacement under flexure and additional deflection owing to shear forces, respectively. On the condition that sandwich composite is comprised of two composite skins (facings), Birman and Bert [33] recommended taking α equal to 1. Hence, the maximum displacement at the middle of the sandwich structure for three-point bending can be obtained using the equation as follows:

$$y_{\max} = \frac{Pl^3}{48EI} + \frac{Pl}{4AG} \quad (6)$$

In order to determine the sandwich beam shear properties and calculate the core shear modulus, the following three equations (7-9) were used according to ASTM D:7250/D7250M – 06 [34]. The equations are valid if the facings are identical, and a single loading configuration test is carried out.

$$D = \frac{E_f(d^3 - c^3)b}{12} \quad (7)$$

$$U = \frac{P(S - L)}{4 \left[\Delta - \frac{P(2S - 3SL^2 + L^3)}{96D} \right]} \quad (8)$$

$$G = \frac{U(d - 2t)}{(d - t)^2 b} \quad (9)$$

Where D is flexural stiffness (N.mm²), U is transverse shear rigidity, S is support span length (mm), L is the load span length which is 0 for three-point mid-span configuration), Δ is the beam mid-span deflection (mm) and G is core shear modulus (MPa).

Bending force vs. deflection curves of sandwich bio-composite obtained from the experiment, Euler-Bernoulli model and Timoshenko model are presented in Figure 8. The prediction from Euler-Bernoulli model was found to underestimate the deflection of the sandwich structure, which is ascribed by the neglect of the displacement occurred by the shear effect. This model provides inaccurate estimation when the core shear modulus is low as the core material is the primary element which bears the shear loads [17]. However, when deflection caused by shear loads were taken into account (Timoshenko model), the model gave greater prediction with the experimental flexure in the elastic phase of the curve. This emphasizes that shear forces cannot be disregarded for this sort of sandwich structures. Similarly, it was reported that for paper reinforced epoxy sandwich composites with aramid honeycomb core [35] and for jute fiber reinforced composite structure with PP honeycomb core [17], Timoshenko model provided good agreements with the experiment that the Euler-Bernoulli theory. Timoshenko model is even more prominent and provides better agreement with the experiment when no significant amount of delamination occurs under the flexural loading, which was the case for our composite panel.

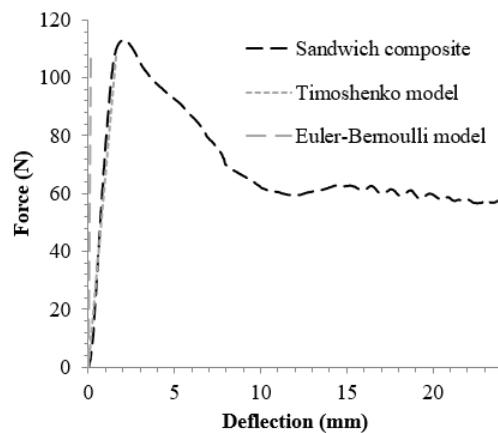


Figure 17. Force-deflection behavior of sandwich composite as obtained from the experiment and models.

4.2. Tensile behavior of composites

Tensile test was also carried out to investigate the effect of the addition of the regenerated man-made cellulose fabrics into the bio-based PP and the influence of incorporation of the PP in the form of pellets in the composites. It was revealed that the rayon fabric PP-sheet composite substantially enhanced the tensile properties as compared to those of neat bio-based PP, and it demonstrates the reinforcing effect of man-made cellulose fabrics. For the tensile strength, the values increased from 20 MPa to 98 MPa, proving 390 % improvement (Table 3). The Young's modulus was seen to improve from 1.12 GPa to 3.1 GPa showing nearly 177 % enhancement. These results can be ascribed to the superior tensile performance of the rayon fabrics. The reinforcing effect was also significant on the ductility of the composite, and the inclusion of rayon fabrics into the PP polymer was found to considerably increase the elongation to break from 6% to 32%.

However, the combination of PP pellets and rayon fabrics could not reach the level of tensile properties of those of rayon PP film composite counterpart. When the bio-based PP was utilised in the form of pellet to make the rayon fiber PP composites, all tensile properties showed an apparent decrease in particular modulus relative to those of rayon fiber composite made of the PP sheets. The modulus, strength and elongation to break were recorded 2.5 GPa, 93 MPa and 30 %. This demonstrated the importance of uniform thermoplastic distribution and impregnation throughout the fabrics.

Johanson et al. [1] studied the tensile strength and modulus of wetlaid lyocell PP composites produced using a hot press, and the tensile strength reported was 29% lower than that of rayon PP sheet composites investigated in the current study at the same fiber mass fraction whereas nearly the same modulus was recorded for the lyocell PP composite and rayon reinforced bio-based PP composite counterpart. The difference between the elongation break values were substantial, and the value of rayon PP composite from this study was found to be 75 % higher that of wetlaid lyocell PP composite.

Table 4. Tensile properties of the bio-based PP and rayon composites.

| Samples | strength (MPa) | elongation to break % | modulus (GPa) |
|-----------------|----------------|--------------------------|---------------|
| rayon pp pellet | 93 | 30 | 2.5 |
| rayon pp sheet | 98 | 32 | 3.1 |
| PP | ~20 | ~6 | 1.12 |

4.3. Impact test analysis

4.3.1. Force- displacement behaviors

Displacement versus force curves obtained from the drop test for sandwich bio-composite and balsa wood samples are depicted in Figure 9.

From the curves of the sandwich composite specimens, stable propagation of the force with respect to the displacement can be found. The average maximum force was recorded 6051.53 N at the depth of 7 mm (Table 4) whereas the force-displacement behavior was different for the balsa wood specimens. The force had sort of unstable trend indicating the weight penetration in the specimen, fracture and tear as illustrated in Figure 10. Without the presence of composite skins, it was observed that the balsa wood core demonstrated a very small maximum force of 75.98 N at the depth of approximately 2.25 mm as compared to that of the sandwich bio-composite. The maximum force was recorded almost 80 times higher for the sandwich composite specimens.

The images (Figure 10) illustrate that unlike wooden samples, which failed completely, and the incident energy penetrated the wood, the sandwich composite specimens were observed to perforate significantly lesser (Figure 10) (c) and (d). This could be concluded that sandwich composites resist failure by dissipating and absorbing energy.

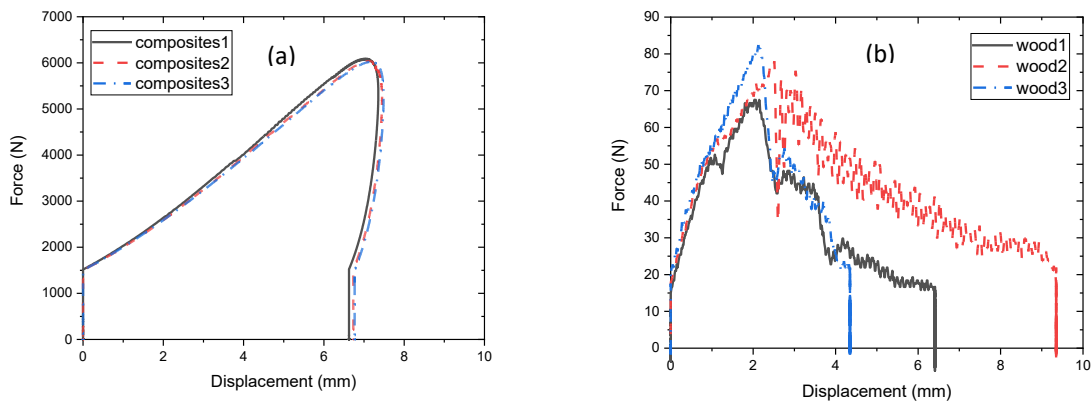


Figure 18. Force-displacement curves for (a) sandwich composite and (b) balsa wood specimens.

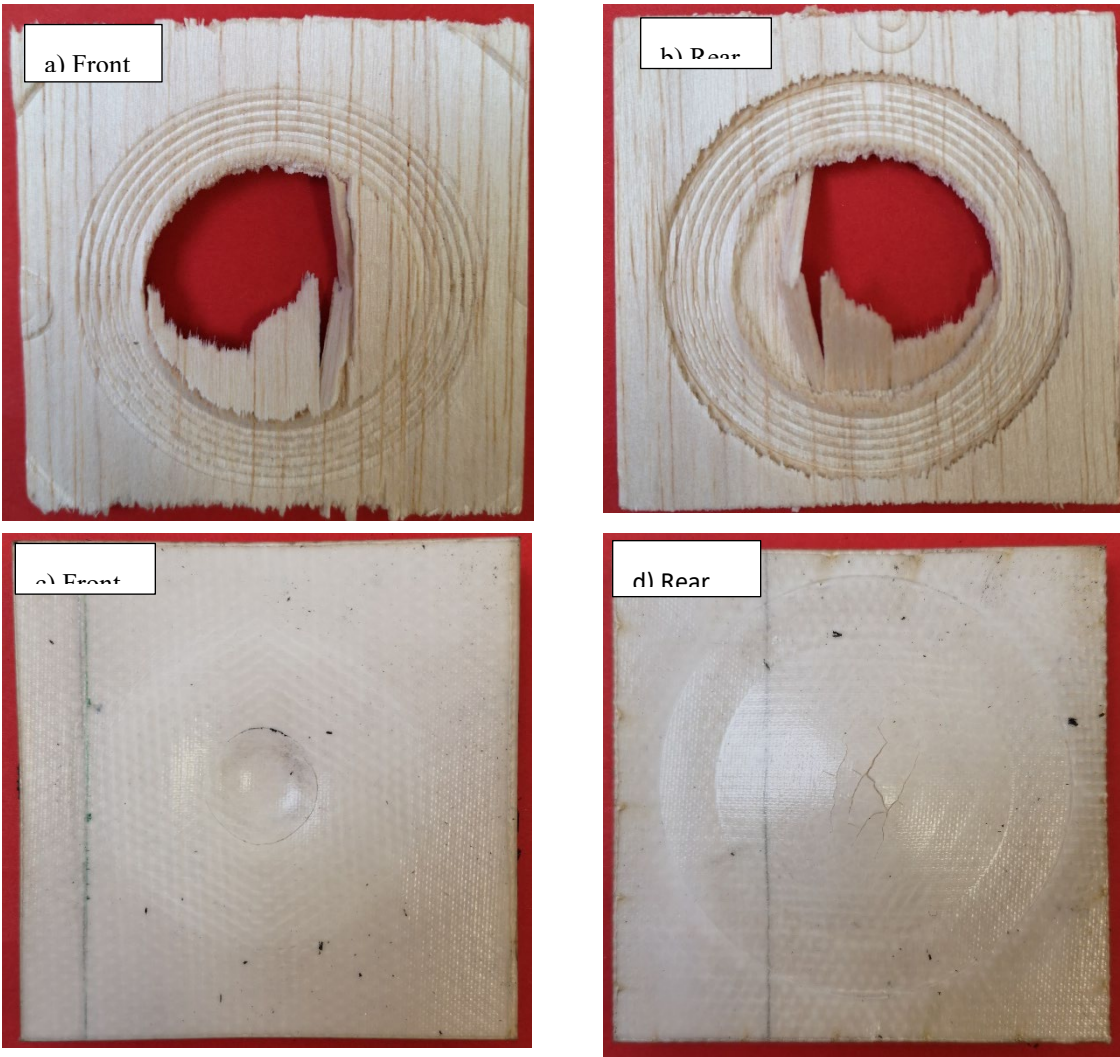


Figure 19. Visual images demonstrating damage patterns of the specimens: (a) wood (front face), (b) wood (rear face), (c) sandwich composite (front face) and (d) sandwich composite (rear face) after the drop test.

4.3.2. Force-time behaviors

The force-time results corresponding to the impact scenario for both balsa wood and sandwich bio-composites are shown in Figure 11 (a) and (b). The force plotted is reaction force exerted by the samples to the impactor tip. The sandwich composites were seen to demonstrate a mountain-like trend similar to parabolic whereas the force-time behavior was different for the balsa wood. A very sharp increase to the ultimate force was observed after around 23 ms contact with the impactor, followed by a prompt load drop due to easy fracture of balsa wood grains, however, it took approximately 35 ms for the sandwich

specimens to reach the maximum force. This proves the significant improvement of impact resistance in the sandwich composites, and that the initial damage and fracture occurred over a longer period.

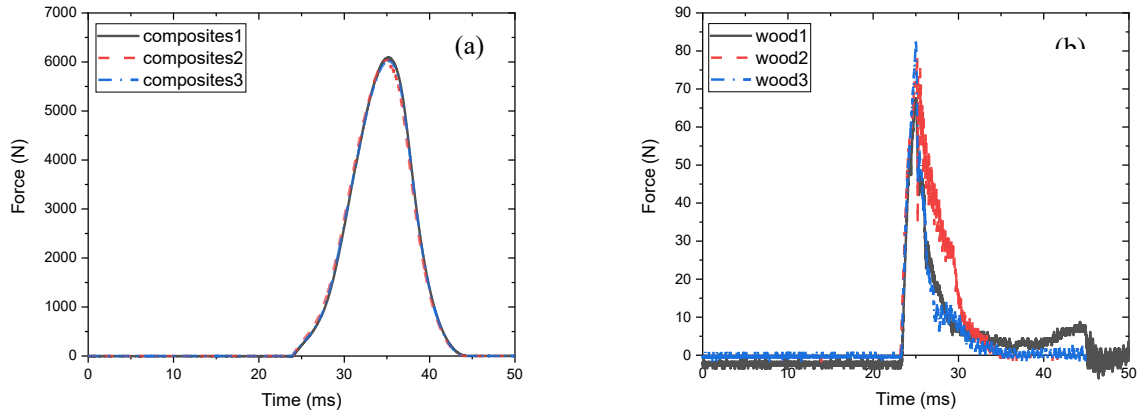


Figure 20. Force versus time curves of the sandwich specimens and balsa wood samples.

4.3.3. Energy-time behaviors

The absorbed energy- time curves are depicted for the sandwich composite and the balsa wood specimens. It was revealed that the enhancement of impact energy was substantial with the incorporation of the bio-based composite skins (Figure 12 (a) and (b)). It was found that the maximum energy improved by 98 times when the sandwich composites were tested. The balsa wood specimens were entirely penetrated (Figure 10 (a) and (b)), allowing the energy to pass through the balsa wood, and therefore, a small amount of energy (0.29 J) was absorbed. However, upon the incident energy of 25 J, the sandwich composite specimens did not puncture, and the maximum energy was recorded 28.37 J for the sandwich bio-composites.

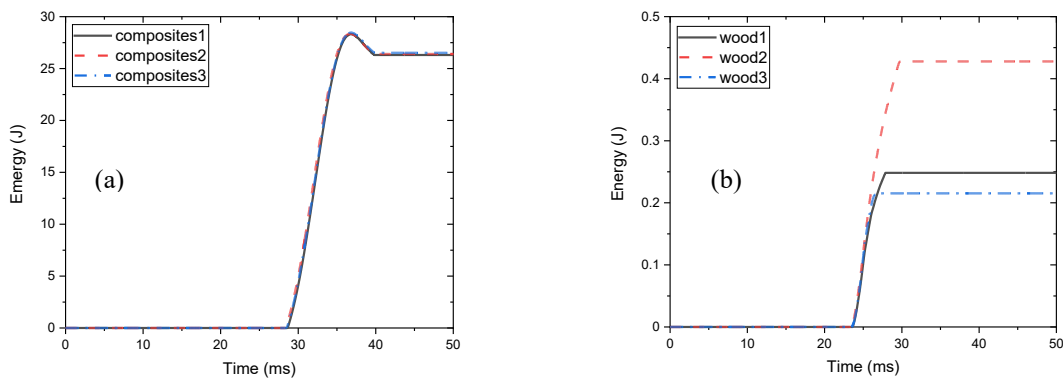


Figure 21. Energy vs. time for (a) the sandwich composite and (b) the balsa wood samples.

Table 5. Average drop test results for the wood and sandwich composites.

| Specimens | Average Maximum Energy (J) | SD (J) | Average Maximum Force (N) | SD (N) |
|--------------------|----------------------------|--------|---------------------------|--------|
| Wood | 0.29 | 0.11 | 75.98 | 7.6 |
| Sandwich Composite | 28.37 | 0.07 | 6051.5 | 30.71 |

4.3.4. Failure and damage modes

Post-impact visual inspection for the balsa wood and sandwich composite are illustrated in Figure 10. The balsa wood images (Figure 10 (a) and (b)) present the damage to the wood specimens and full penetration of the impactor as a circular shape chunk was cut out from the samples. For the sandwich composite specimens (Figure 10 (c) and (d)), some cracks are visible. On the front side of the sandwich specimen, a small round crack formed whereas matrix cracking occurred mainly in the middle of the specimen on the rear side.

4.3.5. Scanning electron microscope (SEM) of fractured surface of the sandwich composite and balsa wood specimens

Figure 13 shows SEM images of the sandwich structure and balsa wood after fracture. Figure 13 (a) illustrates the cross-sectional image of the composite facing after the impact test and its separation from the sandwich composite. It can be observed that the fiber breakages, matrix cracking and slight delamination are clear in the facing and are predominant failure modes. For the balsa wood image, as shown in Figure 13 (b), the cross-sectional view of the structure of the balsa wood (the axial grain direction) shows kind of honeycomb pattern of the cells, which could also contribute to the load absorption capacity of resulting sandwich composites.

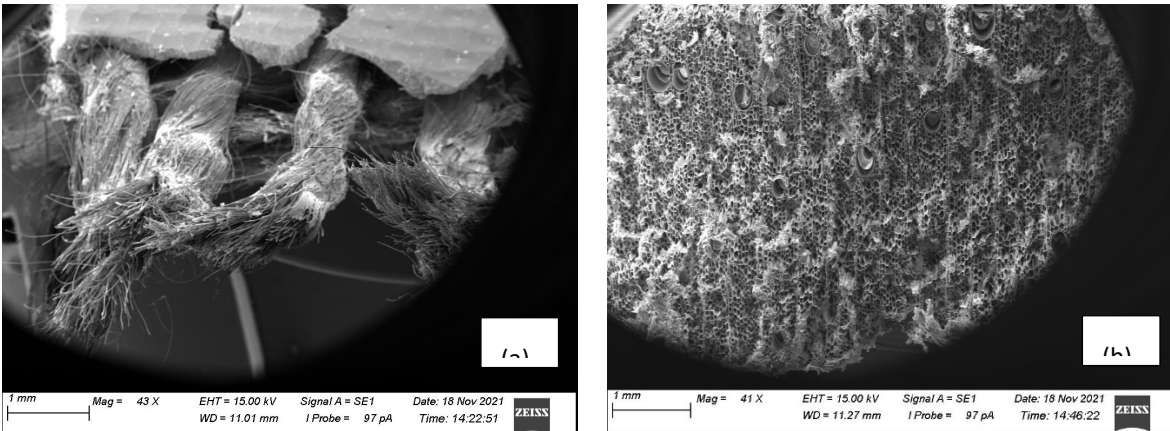


Figure 22. SEM micrographs of (a) the sandwich composite and (b) balsa wood after the impact test.

4.4. Digital imaging analysis

Figure 14 presents the microstructure of the sandwich composite with the PA core material and the facing as well as the rayon PP sheet composite. As observed in Figure 14 (a), good interfacial adhesion between the core and the facing can be observed, as highlighted in the red rectangular. Figure 14 (b) illustrates sufficient bonding between the fabric and PP polymer in the cross-sectional view.

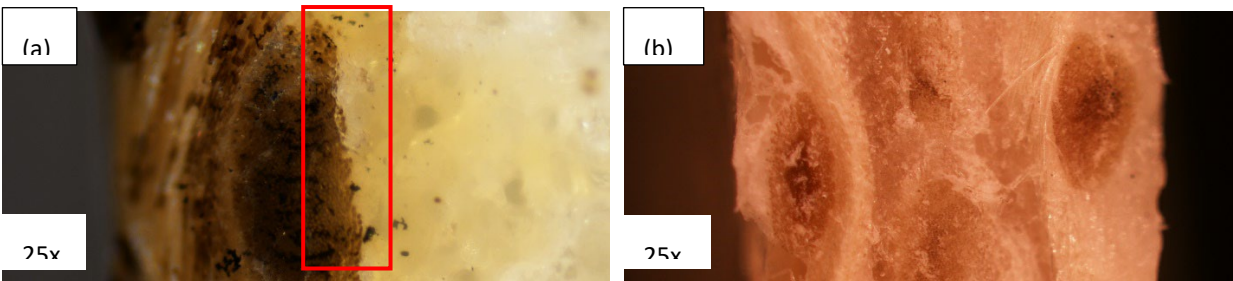


Figure 23. Microscopy images of the interface (a) between the composite skin and PA textile core and (b) between the fibers and bio-based PP at 25x magnification.

4.5. Crystallization and melting behaviours

The DSC thermograms of PP samples in neat PP and composites with the incorporation of PP pellets and PP films are depicted in Figure 18. The crystallization temperature T_c ($^{\circ}\text{C}$), melting temperature T_m ($^{\circ}\text{C}$), crystallization enthalpy ΔH_c (J/g), melting enthalpy ΔH_m (J/g) and degree of crystallinity X_{DSC} (%) are measured and displayed in Table 5. Almost no change was found to detect in all the above-mentioned parameters where the PP was used in the forms of either pellets or sheets in neat PP, rayon PP pellet and rayon PP film. T_c and T_m were obtained around 121-122 $^{\circ}\text{C}$ and 162-163 $^{\circ}\text{C}$, respectively. For the

calculation of the degree of crystallinity, the heat of fusion of pure crystalline PP, ΔH_0 , was taken as 209 J/g [36, 37], and the value of the degree of crystallinity was calculated ca. 36-37 %. This demonstrates that the intrinsic thermal behaviours of the polymer system did not alter with the inclusion of the PP in either form in the neat PP and composites.

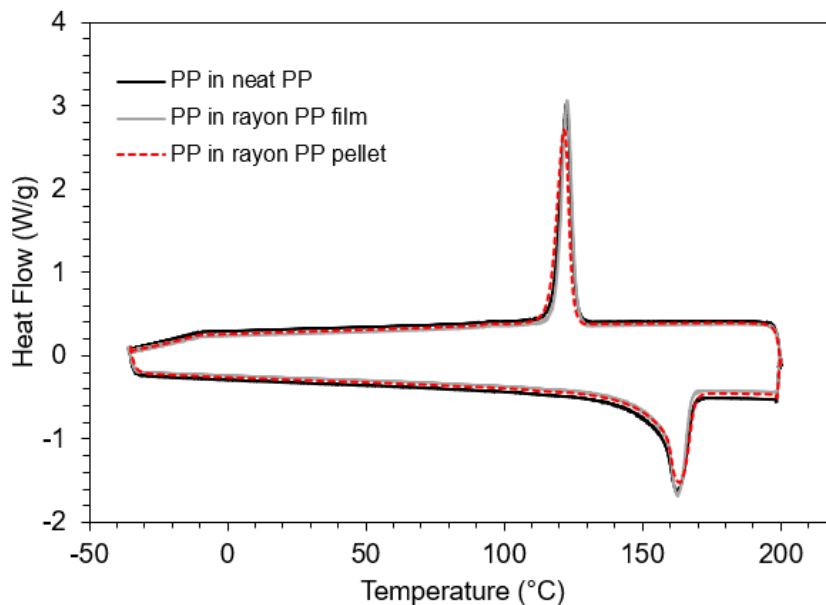


Figure 24. Differential scanning calorimetry (DSC) thermograms of PP in neat PP, rayon PP film and rayon PP pellet.

Table 6. The T_c , T_m , ΔH_c , ΔH_m and X_{DSC} obtained from the DSC measurements for PP in neat PP, rayon PP film and rayon PP pellet.

| Samples | T_c (°C) | T_m (°C) | ΔH_c (J/g) | ΔH_m (J/g) | X_{DSC} (%) |
|--|------------|------------|--------------------|--------------------|---------------|
| Neat PP (in PP plate) | 122.5 | 162.6 | 84.8 | 79.1 | 37.8 |
| PP in the composite in the form of pellets | 121.6 | 163.3 | 84.2 | 77.0 | 36.8 |
| PP in the composite with PP films | 122.7 | 162.8 | 82.8 | 76.8 | 36.7 |

5. Conclusions

The experimental work was designed to study the effect of bio-composite design on the mechanical performance of the composites and the bio-based sandwich composite. The effect of regenerated cellulose fabrics as reinforcement was significant in terms of the improvement of tensile properties and bending modulus as compared to those of neat bio-based PP. The enhancement of flexural properties for both maximum force and initial slope of elastic region was remarkable when balsa core material was used to make sandwich composite system without tangible weight increase. Under the flexure, the sandwich bio-composite samples did not present any evidence of delamination. The bending force-displacement of the sandwich specimens were predicted using the Euler-Bernoulli and Timoshenko models, which the latter theory provides more precise estimation due to the consideration of shear forces in the concept. With the incorporation of the thin regenerated cellulose fibre reinforced bio-based PP composite facings onto the balsa core, the energy absorption and ultimate force of sandwich composites was found to record significantly higher values than the wood after the low velocity drop test. Besides, SEM test analysis was carried out to detect the mode of impact test fracture which was mainly the fiber breakages and matrix cracking. For the future work, it is suggested that film extrusion equipment can be used to provide a more precise and faster solution for the thermoplastic film making process.

Acknowledgments

This research was funded by ÅForsk foundation, grant number 20-412 and knowledge foundation (KK-stiftelsens) fund number 20200142. Special thanks to Cordenka for sponsoring the rayon fabrics.

References

- [1] Johnson RK, Zink-Sharp A, Rennecker SH, Glasser WG. Mechanical properties of wetlaid lyocell and hybrid fiber-reinforced composites with polypropylene. *Composites Part A: Applied Science and Manufacturing*. 2008;39(3):470-7.
- [2] Franciszczak P, Merijs-Meri R, Kalniņš K, Błędzki AK, Zicans J. Short-fibre hybrid polypropylene composites reinforced with PET and Rayon fibres – Effects of SSP and interphase tailoring. *Composite Structures*. 2017;181:121-37.
- [3] Khalili P, Skrifvars M, Ertürk AS. Fabrication, Mechanical Testing and Structural Simulation of Regenerated Cellulose Fabric Elium® Thermoplastic Composite System. *Polymers*. 2021;13(17):2969.

- [4] Khalili P, Blinzler B, Kádár R, Blomqvist P, Sandinge A, Bisschop R, et al. Ramie fabric Elium® composites with flame retardant coating: Flammability, smoke, viscoelastic and mechanical properties. *Composites Part A: Applied Science and Manufacturing*. 2020;137:105986.
- [5] Khalili P, Tshai KY, Kong I. Natural fiber reinforced expandable graphite filled composites: Evaluation of the flame retardancy, thermal and mechanical performances. *Composites Part A: Applied Science and Manufacturing*. 2017;100:194-205.
- [6] Alhijazi M, Safaei B, Zeeshan Q, Asmael M, Eyvazian A, Qin Z. Recent Developments in Luffa Natural Fiber Composites: Review. *Sustainability*. 2020;12(18):7683.
- [7] Mohamad A, Qasim Z, Zhaoye Q, Babak S, Mohammed A. Finite element analysis of natural fibers composites: A review. *Nanotechnology Reviews*. 2020;9(1):853-75.
- [8] Ganster J, Fink HP, Pinnow M. High-tenacity man-made cellulose fibre reinforced thermoplastics – Injection moulding compounds with polypropylene and alternative matrices. *Composites Part A: Applied Science and Manufacturing*. 2006;37(10):1796-804.
- [9] Ganster J, Erdmann J, Fink HP. Biobased composites. *Polimery*. 2013;58(6):423-34.
- [10] Franciszczak P, Bledzki AK. Tailoring of dual-interface in high tenacity PP composites – Toughening with positive hybrid effect. *Composites Part A: Applied Science and Manufacturing*. 2016;83:185-92.
- [11] Khalili P, Kádár R, Skrifvars M, Blinzler B. Impregnation behaviour of regenerated cellulose fabric Elium® composite: Experiment, simulation and analytical solution. *Journal of Materials Research and Technology*. 2021;10:66-73.
- [12] Karian H. *Handbook of polypropylene and polypropylene composites, revised and expanded*: CRC press; 2003.
- [13] Thattai parthasarathy KB, Pillay S, Ning H, Vaidya UK. Process simulation, design and manufacturing of a long fiber thermoplastic composite for mass transit application. *Composites Part A: Applied Science and Manufacturing*. 2008;39(9):1512-21.
- [14] Oliveira PR, May M, Panzera TH, Hiermaier S. Bio-based/green sandwich structures: A review. *Thin-Walled Structures*. 2022;177:109426.
- [15] Grünewald J, Parlevliet P, Altstädt V. Manufacturing of thermoplastic composite sandwich structures: A review of literature. *Journal of Thermoplastic Composite Materials*. 2017;30(4):437-64.

- [16] Davies JM. *Lightweight sandwich construction*: John Wiley & Sons; 2008.
- [17] Karaduman Y, Onal L. Flexural behavior of commingled jute/polypropylene nonwoven fabric reinforced sandwich composites. *Composites Part B: Engineering*. 2016;93:12-25.
- [18] Kolahchi R, Zhu S-P, Keshtegar B, Trung N-T. Dynamic buckling optimization of laminated aircraft conical shells with hybrid nanocomposite material. *Aerospace Science and Technology*. 2020;98:105656.
- [19] Keshtegar B, Farrokhi A, Kolahchi R, Trung N-T. Dynamic stability response of truncated nanocomposite conical shell with magnetostrictive face sheets utilizing higher order theory of sandwich panels. *European Journal of Mechanics - A/Solids*. 2020;82:104010.
- [20] Keshtegar B, Motezaker M, Kolahchi R, Trung N-T. Wave propagation and vibration responses in porous smart nanocomposite sandwich beam resting on Kerr foundation considering structural damping. *Thin-Walled Structures*. 2020;154:106820.
- [21] Motezaker M, Kolahchi R, Rajak DK, Mahmoud SR. Influences of fiber reinforced polymer layer on the dynamic deflection of concrete pipes containing nanoparticle subjected to earthquake load. *Polymer Composites*. 2021;42(8):4073-81.
- [22] Kolahchi R, Keshtegar B, Trung N-T. Optimization of dynamic properties for laminated multiphase nanocomposite sandwich conical shell in thermal and magnetic conditions. *Journal of Sandwich Structures & Materials*. 2021;24(1):643-62.
- [23] Al-Furjan MSH, Yang Y, Farrokhi A, Shen X, Kolahchi R, Rajak DK. Dynamic instability of nanocomposite piezoelectric-leptadenia pyrotechnica rheological elastomer-porous functionally graded materials micro viscoelastic beams at various strain gradient higher-order theories. *Polymer Composites*. 2022;43(1):282-98.
- [24] Sargianis JJ, Kim H-I, Andres E, Suhr J. Sound and vibration damping characteristics in natural material based sandwich composites. *Composite Structures*. 2013;96:538-44.
- [25] Le Duigou A, Deux J-M, Davies P, Baley C. PLLA/flax mat/balsa bio-sandwich—environmental impact and simplified life cycle analysis. *Applied composite materials*. 2012;19(3):363-78.
- [26] Al-Furjan MSH, Shan L, Shen X, Kolahchi R, Rajak DK. Combination of FEM-DQM for nonlinear mechanics of porous GPL-reinforced sandwich nanoplates based on various theories. *Thin-Walled Structures*. 2022;178:109495.

- [27] Al-Furjan MSH, Shan L, Shen X, Zarei MS, Hajmohammad MH, Kolahchi R. A review on fabrication techniques and tensile properties of glass, carbon, and Kevlar fiber reinforced polymeric composites. *Journal of Materials Research and Technology*. 2022;19:2930-59.
- [28] STANDARD B. Fibre-reinforced plastic composites — Determination of flexural properties. BS EN ISO, 14125:1998, +A1:2011
- [29] STANDARD B. Plastics — Determination of tensile properties — Part 4: Test conditions for isotropic and orthotropic fibre-reinforced plastic composites. BS EN ISO 527-4:1997
- [30] Adusumali RB, Reifferscheid M, Weber H, Roeder T, Sixta H, Gindl W. Mechanical properties of regenerated cellulose fibres for composites. *Macromolecular symposia: Wiley Online Library*; 2006. p. 119-25.
- [31] Timoshenko S. *Strength of Materials, Part I, Elementary Theory and Problems* (1955). D. Van Nostrand Company.
- [32] Carlsson LA, Kardomateas GA. *Structural and failure mechanics of sandwich composites*: Springer Science & Business Media; 2011.
- [33] Birman V, Bert CW. On the choice of shear correction factor in sandwich structures. *Journal of Sandwich Structures & Materials*. 2002;4(1):83-95.
- [34] ASTM D:7250/D7250M - 06. *Standard Practice for Determining Sandwich Beam Flexural and Shear Stiffness*. ASTM International.
- [35] Du Y, Yan N, Kortschot MT. Light-weight honeycomb core sandwich panels containing biofiber-reinforced thermoset polymer composite skins: Fabrication and evaluation. *Composites Part B: Engineering*. 2012;43(7):2875-82.
- [36] Li Y, Zhu J, Wei S, Ryu J, Sun L, Guo Z. Poly(propylene)/Graphene Nanoplatelet Nanocomposites: Melt Rheological Behavior and Thermal, Electrical, and Electronic Properties. *Macromolecular Chemistry and Physics*. 2011;212(18):1951-9.
- [37] Brandrup J, Immergut EH, Grulke EA, Abe A, Bloch DR. *Polymer handbook*: Wiley New York; 1999.




Chapter 4

Mechanical Properties of Bio-Based Sandwich Composites Containing Recycled Polymer Textiles



Article

Mechanical Properties of Bio-Based Sandwich Composites Containing Recycled Polymer Textiles

Pooria Khalili ^{1,*}, Mikael Skrifvars ¹, Hom Nath Dhakal ², Saeid Hosseinpour Dashatan ³, Mikael Danielsson ⁴ and Alèxia Feiner Gràcia ⁵

Summery

In this part of the report, sandwich composites were produced by compression moulding techniques, and they consisted of regenerated cellulose fabric (rayon) and bio-based polypropylene (PP) to form facings, while virgin and recycled polyamide (PA) textiles were used as core materials. To compare the mechanical performance between sandwich composites and typical composite designs, a control composite was produced to deliver the same weight and fiber mass fraction from rayon and PP. To evaluate the influence of recycled textile on the mechanical properties of the composites, a series of flexural, low velocity impact (LVI) and tensile tests were performed. It was found that the incorporation of thicker PA textile enhanced the bending stiffness by two times and the peak flexural force by 70% as compared to those of control. Substitution of a layer of recycled textile for two layers of rayon provided a good level of impact energy absorption capacity (~28 J) and maximum force (~4893–5229 N). The tensile strength of the four sandwich composites was reported to be in the range of 34.20 MPa and 46.80 MPa. This value was 91.90 for the control composite. The 2D cross-section slices of the composite specimens did not show any evidence of fiber tow debonding, fiber bundle splitting, or delamination.

1. Introduction

Demand for the utilisation of textile materials has been increasing in different industries, which leads to the accumulation of textile waste. While the rate of recycling is globally lesser than 20%, the rough estimation of the generation of textile waste is higher than 150 million tonnes [1,2]. A large quantity of these wastes is either discarded or incinerated, and this does not have a positive impact on the environment. When these large quantities of textiles

are discarded in landfills as waste, they contaminate groundwater through decomposition and form micro-plastics and greenhouse gases [3]. The ever-growing world population, which brings increased consumption, has resulted in an acute shortage of resources [4,5]. Moreover, the adverse effects of synthetic waste materials are vast, ascribed to their toxicity and non-biodegradability. These factors have directly affected the textile industry and demonstrate the importance of recycling textile waste [6].

An enormous quantity of textile waste is generated in the paper, pulp, and textile industries throughout the production process. Rejected fabrics, fabric scraps, cutting waste, yarns, threads, and short fibers are major wastes in varying sections [7]. These textiles are greatly engineered textile structures composed of yarns of polyamides and polyester and are wove into various types of textile structures. Rather than disposing of textile materials and incinerating them after their life span, cleaning processes and various treatments can be performed on the textiles in order to utilise them as rein-forcements for specific composite applications.

Use of recycled textiles contributes to reducing the creation of new fibrous materials through agricultural approaches and extraction, which lead to a higher carbon footprint. By valorizing the recycled textiles, there is a reduction in negative environmental im-pacts caused by discarding waste in the form of textiles [3].

Owing to damage, wear, and other issues, textile waste produced nowadays cannot be reused in production lines for consumer products. However, post-consumer waste possesses the potential to be utilised for diverse purposes, where its properties and performance can be utilised and enhanced.

In the paper machine, textile materials are called paper machine clothing and are used for the formation and dewatering of the pulp. The life span of these textiles is typically from 30 days to 90 days, depending on the position in the machine and the paper grade. After a full life cycle, the machine's clothing must be replaced. There is therefore an interest in studying various ways to recycle or reuse these textiles as sec-ondary products. The textile still retains good properties, such as strength and durability, which could be used in composite structures. Manufacturing semi-structural composite materials using textile waste is one of the most useful recycling methods that is sus-tainable.

Man-made regenerated fibers have been revealed to offer significant promise as reinforcements in thermoplastics for continuous [8] and short fiber systems [9,10]. They provide CO₂ neutrality, low density, biodegradability, and non-

abrasiveness to manu-facturing equipment, the same as natural fibers (NFs) [11,12]. In addition to these characteristics, they possess the uniform morphological structure, mechanical properties, and physical properties of synthetic fibers. Varying manufacturing techniques can be used to produce man-made regenerated fiber (rayon) thermoplastic composites, such as compression moulding, resin infusion [8,13], and injection moulding [10,14,15]. The flexural strength and modulus of rayon Elium® composites obtained from the infusion technique were 93.5 MPa and 5.6 GPa, respectively [8]. The flexural modulus of rayon fiber PP composites after injection moulding was 3.88 GPa) [10].

Because of the lowest density and competitive price of polypropylene (PP) among other polymers, PP is known as a commonly used polymer [16]. PP is also chemical, bi-ological, water-resistant, fatigue-resistant, and possesses insulating properties, and is recyclable. Therefore, the combination of PP and rayon fibers can offer a suitable fit for the requirements of lightweight applications. The construction of composites made from PP and rayon fibers can be altered to meet the needed requirements. Sandwich structures are one of the typical types of panels that provide a high bending stiff-ness-to-weight-ratio and are suitable to be used in key application areas such as marine, transport, sports, and leisure. An investigation [17] was carried out to study sandwich composites made from viscose fabrics and unsaturated polyester. Non-woven layers of viscose fabrics were used as the core material, while the warp knitted viscose fabrics were used as skin layers. Specimens were subjected to an incident energy of 25 J, and the structures with more warp knitted fabrics were found to reveal a greater impact force.

The aim of this project was to investigate and develop methods for recycling and reusing recycled paper machine textiles after their end-of-life as a component in a composite material. Due to its excellent mechanical properties, the textile could have a potential use in structural composites. These could be sandwich composites, in which the paper machine textile is used as the core material. The recycled textiles as core materials have the potential to withstand higher bending forces and induce greater stiffness than those of the bio-based composite materials. The inclusion of recycled textiles can not only improve the mechanical performance, but it can also make the composite part less expensive. To the best of the authors' knowledge, very few reports [17] have studied the use of regenerated cellulose fibers in sandwich composites. Moreover, the utilisation of PP containing bio-based content to make sandwich composites has not been reported. Incorporation of recycled textiles in the regenerated cellulose fiber bio-based PP

composite construction has not been introduced thus far. Therefore, in this work, the effects of the inclusion of various virgin/recycled polyamide (PA) textile fabrics into the rayon bio-based PP composite on the flexural, tensile, and low-velocity impact performance were investigated. The modes of failure of the sandwich specimens were also studied using an X-ray micro-computer tomography (μ CT) image test with high-resolution images. The new class of sustainable sandwich composites investigated in this study can be utilised as lightweight composite structures suitable for various applications.

2. Materials and Methods

2.1. Materials

Regenerated cellulose fabrics (rayon) 0/90 were supplied by Cordenka company, Germany. The grade was 700 2440 dtex, with a density and area weight of 2482 dtex and 442 g/m², respectively. The polymers used were bio-based polypropylene (PP) purchased from NaturePlast, France, and had 30 wt% bio content. The PP manufacturer provided the melt flow index (230 °C) and density of 70 g/10 min and 0.9 g/cm³, respectively. Paper machine textiles (felts) were provided by Albany International, Sweden. Felts were made of polyamide (PA) and supplied in both virgin and used forms. The textile acts as a sub-strate/support on which the pulp is formed into the paper product. These textiles are used under very demanding conditions, and they are highly engineered textile structures composed of yarns. Compaction of the felt, or loss of void volume, with time reduces the dewatering capacity of the felt, which is the main reason for its limited life or why felts are exchanged on a rather frequent basis. Moreover, the felt is subjected to various conditioning processes that wear the felt, resulting in fiber loss. Regarding the discoloration of felts after pulp and paper processing, it can be added that felts originally had a white colour. Discoloration relates to the process, or rather, the chemistry involved. The blue felt comes from a mill adding UV-light absorbents or whitening agents, which are most often blue. The brown roll is from another mill where pulp containing lignin is used. Before further processing, the used PA felts were washed thoroughly using lukewarm water for some minutes, rubbed simultaneously with hands to eliminate the impurities, and subsequently dried in a convection oven for 24 h at a temperature of 90 °C.

2.2. Processing

PP pellets were first used to make films of 0.25 mm thickness using a 20-tonne bench press machine (Rondol Industrie SAS, Nancy, France). The process conditions were optimised, as reported in our previous work [18]. To obtain the required thickness, 5 g of PP pellets were pre-heated at 200 °C between the top and bottom press plates for 1 min and subsequently pressed under the press area measuring 190 mm (length) × 190 mm (width) at 5 kN compressive force and the same temperature for another minute. The films were eventually cooled down for 3 min at room temperature and collected for composite manufacturing.

A film-stacking system was constructed by placing the alternative rayon fabrics, felt, and PP films to produce the sandwich composites with the aid of the same hydraulic press equipment that was used in the film-making process. A similar approach was carried out in our previous publication [18]. In fact, four thin PP film layers were utilised to bond the two layers of rayon fabrics to a PA felt (core) middle material, and therefore, the PA was the middle layer in the structure. The whole assembly was prepared for a dimension of 180 mm × 180 mm and then was pressed for 10 min at a pressure of 0.1 MPa and a temperature of 200 °C. Afterwards, the assembly was cooled down for 30 min at room temperature. It should be noted that the previously cut layers of rayon fabrics were dried in a convection oven for 24 h at 70 °C prior to the composite fabrications to eliminate the moisture content of the fibers.

Four different types of felt middle layers were used to form four distinct sandwich composites. The purpose was to examine the effect of varying thicknesses and recycled textiles obtained from different processes, which resulted in different types of contamination, on the mechanical behaviours of the sandwich composites. The use of waste textiles as a middle layer eliminates the probability of contamination since it is covered by top and bottom skins. In addition, they have porous structures that can act as core materials. When the virgin thick felt was used as the core layer, the composite was designated as VTC with a thickness of 5.0 mm. The composite with the virgin thin felt measuring 3.9 mm as the core layer was designated as VtC. The sandwich composites containing recycled felt materials were named brown core composite (BC) and blue core composite (BIC) and had the same thickness of 3.9 mm. The thin virgin felt and two used felts had a thickness of 2.6 mm, and the thickness of the thicker virgin felt was measured at 3.9 mm (Table 1).

In order to appropriately compare the results, in particular the bending behaviours, a control composite (C) possessing nearly the same weight as the sandwich structures containing the thinner cores was produced. Two layers of PP films were positioned between each of the two layers of fabrics (in total, four layers of fibers were incorporated), and on the very top and bottom layers of laminate, only one PP film was placed. The processing conditions, i.e., temperature, time, and pressure, of the composite laminate were identical to those carried out for the sandwich structures. The fiber mass fraction was determined to be approximately 50% for both the composite skin of the sandwich structures and the control composite. It is worth mentioning that the PP mass fraction in the whole sandwich composite containing the thinner cores is calculated at 27%. The composite plates were then cut into the required dimensions using a piece of laser cutting equipment (a GCC Laserpro Spirit GLS instrument) for different testing in accordance with the standards. Directly before the tests, the samples were conditioned for 24 h in a humidity chamber set to a temperature of 23 °C and a relative humidity of 50%.

Table 1. Composite formulations.

| Sample | Impurities of the Textile Core before Cleaning | Type of Felt | Thickness of Felt (mm) | Thickness (mm) |
|--|--|--------------|------------------------|----------------|
| Composite with a virgin thick core (VTC) | No contamination | virgin | 4 | 5 |
| Composite with a virgin thin core (VtC) | No contamination | virgin | 2.6 | 3.9 |
| Composite with a blue core (BIC) | UV light absorbents or whitening agents | used | 2.6 | 3.9 |
| Composite with a brown core (BC) | Pulp containing lignin | used | 2.6 | 3.9 |
| Control (C) | NA | not used | 2.6 | 3.9 |

2.3. Mechanical Properties and Damage Characterisations

The flexural tests were carried out on a Tinius Olsen H10KT universal testing instrument in accordance with the BS EN ISO 14125 standard. For these three-point bending tests, the loadcell of 250 N was connected to the equipment,

and the crosshead speed of 5 mm/min was used to apply the load to the samples measuring 80 mm (length) × 20 mm (width) in dimension. A span length of 64 mm was used. A total of five specimens were tested for each composite laminate, and the average values of flexural strength and modulus were reported for the composite plates, and the average values of bending force, initial slope of force-displacement curves, and displacements at maximum force were recorded for the sandwich composites.

The low velocity impact (LVI) experiments were carried out using the Instron CEAST 9340 drop weight machine. The experiments started by applying 15 Joules (J) incident energy to VTC. However, this amount of energy was not sufficient to damage or deform the sample. The incident impact energy was then increased from 15 J to 25 J, and this impact energy value was utilised to be applied to all the samples. The tests were carried out at room temperature, and all the tests were conducted in identical conditions. The LVI tests were conducted for five different types of materials, namely, VTC, VtC, BC, BIC, and control composite, and four specimens were tested for each material. The length and width of the LVI specimens were 70 mm × 70 mm. Force-displacement, force-time, and energy-time traces obtained from LVI tests were utilised to quantify and compare the impact response of these materials.

The tensile tests were performed with the same universal testing machine used for the flexural testing on all the composite laminates according to EN ISO 527-4 (type 1B specimen). The dog bone samples were cut using the laser machine and were tested at a crosshead speed of 2 mm/min and a span length of 50 mm. A loadcell of 5 kN was used, and a 100R mechanical extensometer was connected to the middle of the samples possessing the initial distance between grips of 115 mm. The test was performed on five specimens of each composite, and the average values of tensile strength, modulus, and elongation at break were then reported.

An x-ray micro-computer tomography (μ CT) image test was performed to investigate the failure of the test specimens after the LVI tests. A Nikon XTH 225 was used to scan the damage and the volume graphics VGSTUDIO MAX software (Version 2022.4) was used to render the 3D reconstructed volume. The micro-computer tomography (μ -CT) unit was set to an accelerating voltage of 135 kV and a beam current of 120 μ A with no filtering and a molybdenum target metal. The unit is fitted with a Perkins Elmer flat panel detector. The resulting voxel size was 0.088 mm, and a

total of 3600 images (with 0.1-degree intervals) were taken to produce the 3D reconstructed volume. The resulting images were processed on another computer to obtain the tomography images.

Digital imaging microscope tests were carried out to determine the bond strength between the inner core and the outer composite layer of the sandwich panels, as well as between the layers of fabric and the bio-based PP in the rayon composite laminate (control). A Nikon eclipse LV150 N microscope with a sophisticated optical system and digital imaging capabilities was used to examine the samples. Cross-sectional images of the samples were taken without any surface coating, enabling a thorough analysis of the bond quality at a microscopic scale.

3. Results

3.1. Flexural Properties of Composites

The bending tests were performed to study the effect of thicker, thinner felts as well as recycled felts as core materials on the bending force, displacement, and stiffness of the sandwich composites. The control composite was tested to provide a comparison in terms of flexural behaviours with those of the sandwich composites containing felts. The control and sandwich composites made of thinner cores were produced to offer the same weight for a reasonable evaluation of results (Table 2), except for the composite laminate consisting of thicker felt, which demonstrated a slightly higher weight. The ultimate force was found to be greatest for VTC, attributed to the higher thickness of the felt, which acts as a core material due to its porous structure. For this composite, an approximately 70% increment in the maximum force was obtained as compared to that of the control, which depicts the enhanced load-bearing capacity of the sandwich composite. The ultimate force was found to be lower than VTC for the sandwich composite specimens with thinner felt. Considering the variations in max. force for each composite, the sandwich composites containing thinner felts did not stand out from each other; however, they demonstrated higher values than those of the control.

The increased initial slope of the force displacement (Table 2) of the VTC composite specimens, which can be referred to as the greater stiffness, verified the effectiveness of the incorporation of the thicker core materials in the structure. If a ratio of 1 is given to the initial slope of the force vs. displacement for the control formulation, the stiffness displays 1.3 times more enhancement for BIC and BC sandwiches, 1.8 times more for VtC, and two times more for VTC

composites than that of the control. In this case, the sandwich composites containing recycled cores (BLC and BC) presented a 0.3-time greater stiffness than that of VtC. This can be attributed to the compaction of the PA felts when they were initially used as a substrate in the formation of paper products. They lost their porosity and void volumes and also wore during paper-making processes under those demanding conditions. Displacement wise, the deflection at the maximum force was recorded as 30.2% and 28.8% greater for that of the VTC and sandwich composites with the thinner felt in comparison with that of the control, respectively. This is attributed to the ductility of the PA felts, which contributed to higher displacements, and the value is expected to be higher for the VTC as more PA existed in these specimens.

It was also revealed that all five different types of composites bent after the flexural tests and underwent a plastic deformation; however, no sign of delamination, visual microcracks, or debonding was detected. No indication of a dent in the samples through the flexural indenter was observed in the specimens as well.

Table 2. The flexural properties of the control and sandwich composites.

| Sample | VTC | VtC | BIC | BC | C |
|--|----------------|---------------|---------------|---------------|----------------|
| Thickness (mm) | 5.0 | 3.9 | 3.9 | 3.9 | 2.8 |
| Weight ratio | ~1.1 | ~1 | ~1 | ~1 | 1 |
| Max Force (N) [SD] | 84.4 [1.88] | 71.2 [5.4] | 75.3 [6.7] | 67.3 [2.1] | 49.69 [3.3] |
| Average initial slope (of force-displacement curves) | 33.3 | 30.0 | 21.4 | 21.6 | 16.7 |
| initial slope ratio | ~2.0 | ~1.8 | ~1.3 | ~1.3 | 1.0 |
| Average displacement (mm) [SD] at max. force | 14.9 [0.2] | 13.4 [0.8] | 13.4 [1.0] | 13.4 [0.3] | 10.4 [0.8] |

3.2. Impact Damage Behaviour of Different Composites

The results for each material are presented in terms of force-displacement, force-time, and energy-time graphs and are depicted in Figures 1–3. As seen in these graphs, the specimens in each material group demonstrate similar responses. This implies appropriate repeatability of the experiments. However, as shown in Figure 4, the control composite

sample showed a slight variation compared to the others. Therefore, this sample was not used for making comparisons between different materials.

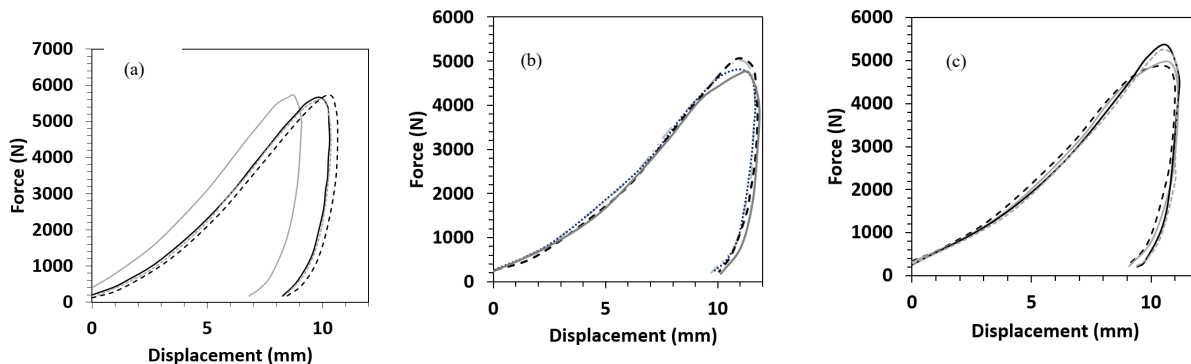


Figure 1. Force-displacement response of (a) Control, (b) VtC, and (c) BC after the impact drop tests on the composites.

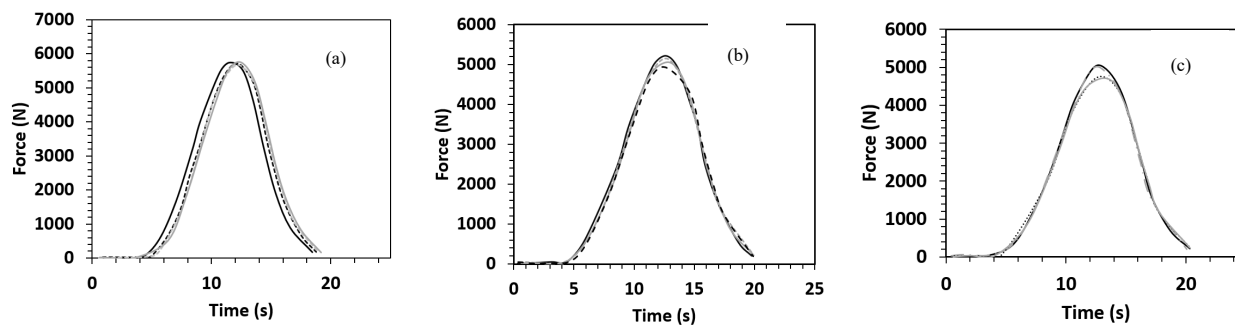


Figure 2. Force-time response of (a) Control, (b) BIC, and (c) VtC after the impact drop tests on the composites.

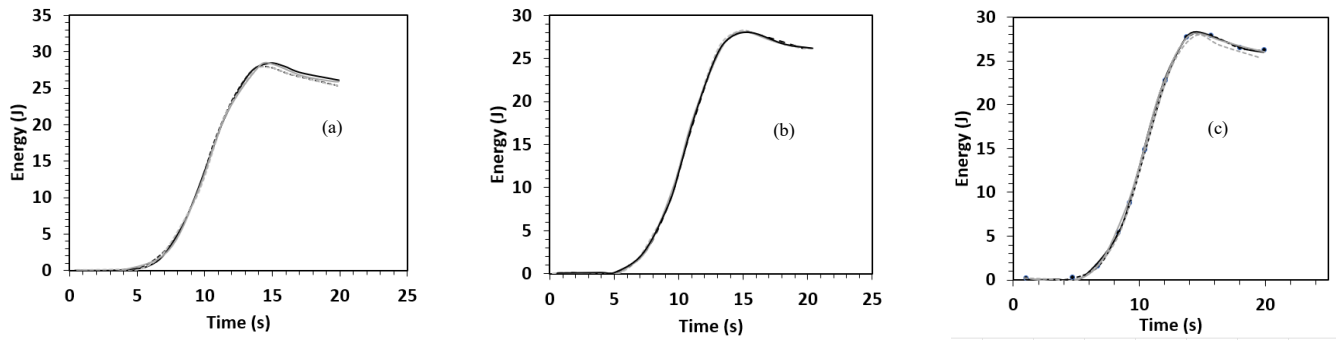


Figure 3. Energy-time response of (a) BIC, (b) VtC, and (c) BC after the impact drop tests on the composites.

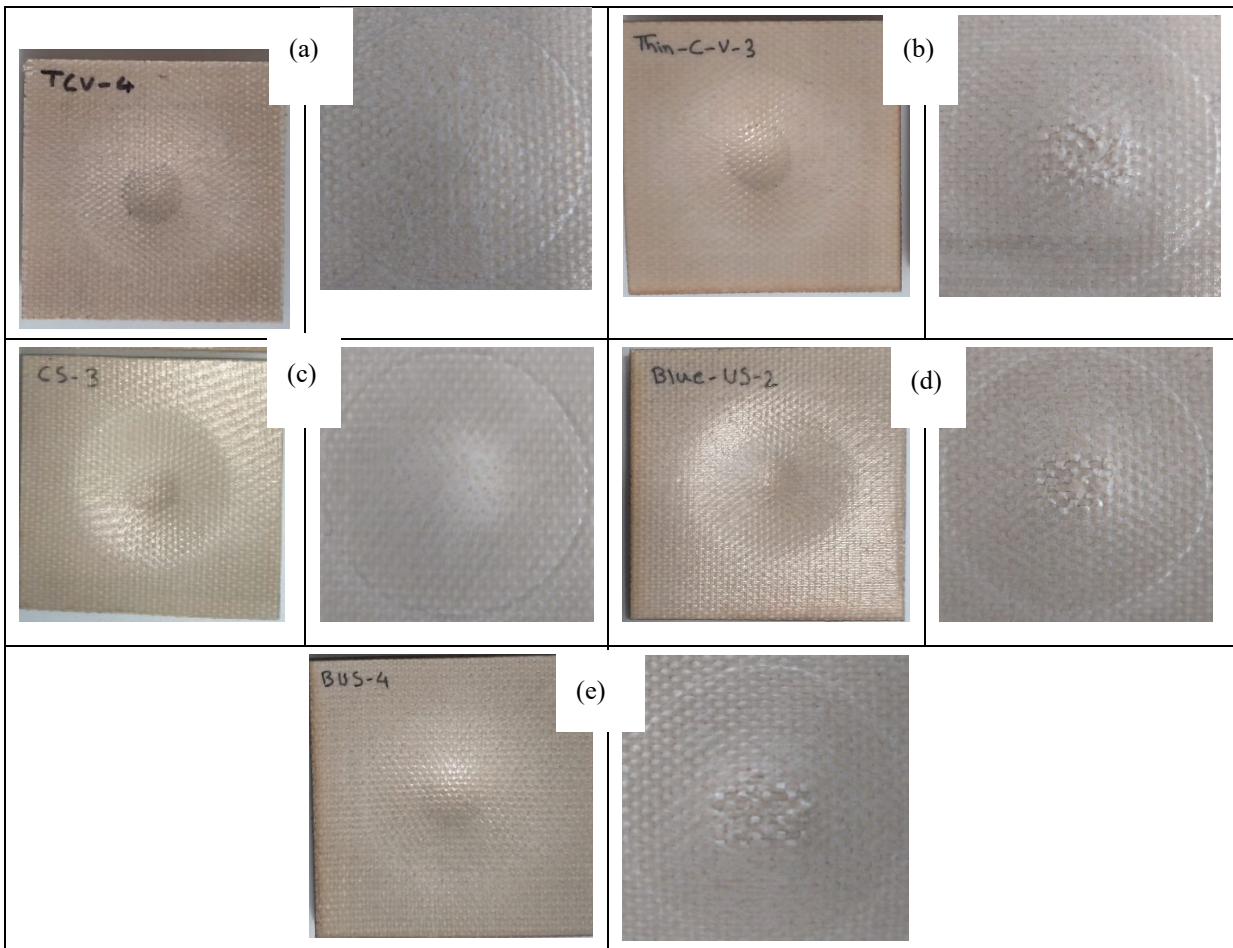


Figure 4. Visual inspection for perforation pattern of the front face of (a) the VTC, (b) VtC, (c) Control, (d) BIC, and (e) BC samples after the impact test (the images on the right side are the close-up versions).

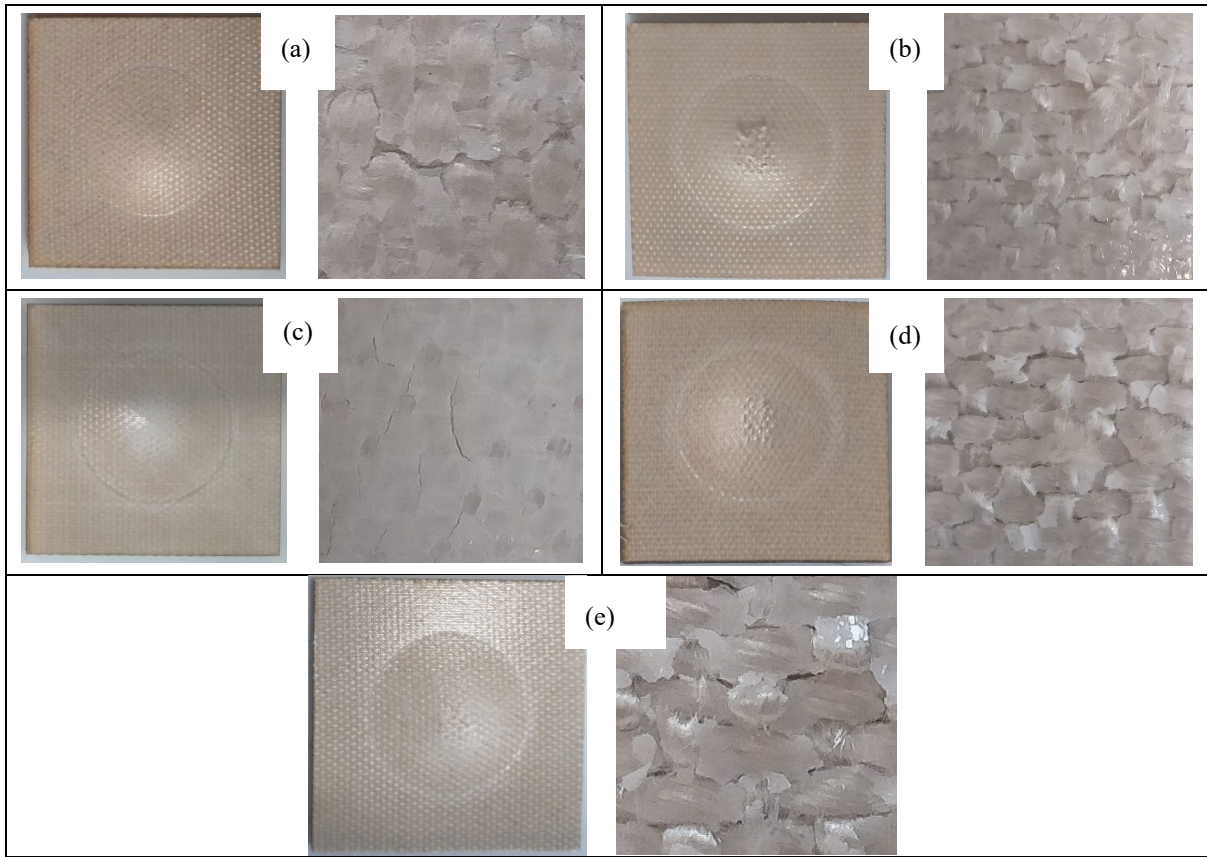


Figure 5. Visual inspection for perforation pattern of the rear side of (a) the VTC, (b) VtC, (c) control, (d) BIC, and (e) BC samples after the impact test (the images on the right side are the close-up versions).

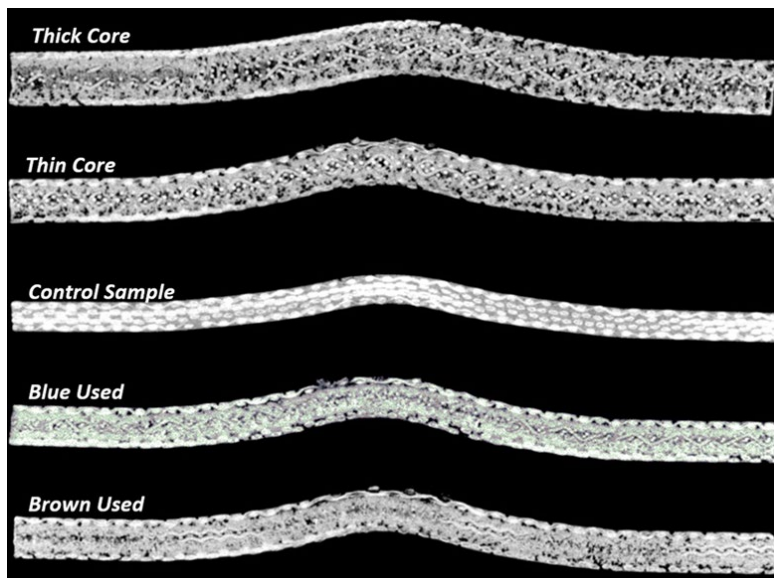


Figure 6. CT images of the composite laminate specimens in impact zone cross-section.

3.2.1. Force-Displacement Response

Force-displacement curves after the drop test for three of the laminates are exhibited in Figure 1a–c, and the summary of the results is shown in Table 3. A very similar relationship can be observed between the force and displacement of all the composite laminates. The highest peak force was recorded at ca. 5229 N for VTC amongst all four sandwich composites, which is attributed to its thicker PA core, followed by BC, BICC, and VtC laminates, which showed the maximum force in the range between approximately 4893 N and 5121 N. Due to the presence of more ductile rayon fabric layers in the control composite, the peak force was found to be at a higher value (5687 N). All the composites were tough, and the incident energy of 15 joules did not make a dent in the samples, and no sign of perforation was detected. Therefore, 25 J of incident energy was introduced to all the composites, and the damaged images of the samples under this impact energy are illustrated in Figures 4 and 5. As seen in Figures 4 and 5, it was observed that the specimens did not delaminate and the drop weight did not penetrate, indicating their failure resistance through energy absorption and dissipation; however, it was detected that the samples were dented in a circular shape on both sides. The force-displacement curves showed the stable propagation of the damage to the samples, and the maximum displacements of all the composite laminates were not very far from each other, falling within the range between 13.01 mm and 14.30 mm. It is promoted that the maximum displacements (Table 3) are in good agreement with the bending displacements at maximum force for the sandwich composite systems. Ude et al. [19] produced sandwich composites with silk-woven epoxy skins together with honeycomb (density = 0.056 kg/m³) as well as polymeric foam (0.052 kg/m³) as core material. The composite specimens were tested under an incident energy of 48 J, and it was revealed that sandwich composites with the honeycomb core and foam recorded peak forces of 800 N and 900 N, respectively. Another investigation [20] was performed on the sandwich composites with flax fiber epoxy composite skins and high-density polyethylene bottle caps as core materials. The peak force obtained from the drop test under an incident energy of 50 J was 1900 N. Hachemane et al. [21] made jute fiber epoxy composite skins and bonded them to cork agglomerate cores to produce sandwich composites. Under the impact energy of 16 J, the sandwich composite containing cork agglomerate cores with densities of 270 kg/m³ and 310 kg/m³ was found to demonstrate a peak force of 2700 N and 2000 N, respectively. It is worth mentioning that the peak forces obtained from the sandwich composite

specimens with PA cores in this study presented higher values than the above-mentioned ones collected from the literature.

Table 3. Average drop weight impact test results for the control and sandwich composites.

| Specimens | Average Maximum Energy (J) | SD (J) | Average Maximum Force (N) | SD (N) | Max. Displacement (mm) | SD (mm) |
|-----------|----------------------------|--------|---------------------------|--------|------------------------|---------|
| Control | 28.13 | 0.02 | 5687.83 | 47.21 | 13.01 | 0.18 |
| VtC | 28.32 | 0.014 | 4893.21 | 158.07 | 14.30 | 0.09 |
| BC | 28.16 | 0.14 | 5121.07 | 224.47 | 13.70 | 0.09 |
| VTC | 28.13 | 0.27 | 5229.23 | 69.34 | 13.96 | 0.56 |
| BIC | 28.06 | 0.19 | 5061.94 | 102.16 | 13.79 | 0.21 |

3.2.2. Force-Time Behaviours

The force-time curves corresponding to the low velocity impact event for the composite specimens are presented in Figure 2a–c, and their respective parameters are shown in Table 3. The force is obtained as the reaction force exerted by the sample on the impactor tip. The force-time curves of all the composite specimens illustrated a mountain-like trend, nearly parabolic. In the case of thicker PA core material, the height of mountain-like curves improved as compared to other sandwich composites. Moreover, it was found out that the time to reach peak force was longer for this VTC sandwich composite than all other composites. The VtC, BC, and BIC sandwich composite specimens were found to reveal very close values of the time to peak force, which can be attributed to the same thickness of the sandwich composites in their structures. It is worth highlighting that the time taken to end the impact scenario was longer ($t \geq 20$ ms) for all the sandwich composites than that of control ($t < 20$ ms).

3.2.3. Energy-Time Behaviours

The energy-time curves corresponding to the drop event for all the composites are depicted in Figure 3. At the incident energy of 25 J, the bio-based composite laminates were not punctured completely. This infers that the energy was absorbed and did not pass through the specimens. Moreover, it was figured out that all the sandwich composites and

control demonstrated the same level of impact energy absorption, and the ultimate energy was recorded at about 28 J.

3.2.4. Impact Damage and Failure Modes

The visual images taken from the post-impact tests are depicted in Figures 4 and 5. Damage patterns on the top surfaces of the composite laminates showed clear matrix cracking (Figure 4), and the damage was more pronounced for the sandwich composites with the thinner core (VtC, BC, and BIC). However, VTC and Control were observed to experience less damage, as it is clearer in the close-up images.

The composite specimens detected did not show fiber pull-out, fiber breakage, and delamination. The damage propagation of the composite specimens was seen to be very similar. A circular-like effect was obvious on the front face of the specimens, where the spread of the impacted energy can be detected.

As seen in Figure 5 (close-up views), matrix cracking and damage propagation were more conspicuous in the sandwich composites containing thinner PA cores (VtC, BC, and BIC). These sandwich composite specimens were found visually to be very similar in their failure patterns owing to their similar composite configurations. In the case of VTC, less deformation and fewer cracks were observed upon impact, implying that the sandwich composite with a thicker core was more impact resistant due to the greater absorption of the energy dissipation.

The X-ray micro-CT images of the specimens after the impact tests are illustrated in Figure 6. The deformation mechanisms of the composite samples in the area of cross-section are illustrated in the CT images. No fiber bundle breakage, tow debonding, fiber bundle splitting, or delamination could be found in the 2D cross-section slices of the composite specimens. Moreover, no obvious cracks were observed directly underneath the contact zone. In other studies, the X-ray micro-CT tests were performed on carbon-epoxy-based composites [22,23], and similar modes of failure were observed for the plain carbon fabric-reinforced epoxy composite specimens at an impact energy of 35 J [22].

3.3. Tensile Test Analysis of the Composites

The tensile strength and modulus of the composite laminates are shown in Table 4. The control specimen was found to demonstrate tensile strength and modulus of 91.90 MPa and 1.35 GPa, respectively. When the sandwich composite samples were pulled from the ends, it was detected that the tensile strength decreased to a value range of approximately 34–46 MPa. Similarly, the tensile modulus was seen to drop to a lower value of 0.36–0.67 GPa as compared to that of control. The reasoning behind these is that more (rayon) fibers existed in the control composite, which led to higher properties of the composite in the tension mode, given the fact that the tensile test is a fiber-dependent characterisation. Moreover, since the sandwich structures possessed a cellular-like structure with numerous amounts of porosity, a direct calculation of tensile strength and modulus is expected to be lower as compared to that of the control. Furthermore, the presence of porous core material, as expected, reduced the tensile modulus as the through thickness was not fully covered by the PA material. Moreover, PA has a lower modulus than rayon fibers, as the current grade of rayon fiber has a 14.3 GPa tensile modulus. VTC was seen to have a lower tensile modulus among other composites, attributed to its thicker PA core material.

Table 4. Tensile strength and modulus of the sandwich composites and Control.

| Materials | Strength (MPa) | SD (Strength) | Tensile Modulus (GPa) | SD (Tensile Modulus) |
|-----------------------------------|----------------|---------------|-----------------------|----------------------|
| Control (C) | 91.90 | 0.80 | 1.35 | 0.05 |
| Virgin thin core composite (VtC) | 34.20 | 1.80 | 0.56 | 0.01 |
| Brown core composite (BC) | 45.70 | 1.80 | 0.49 | 0.01 |
| Virgin thick core composite (VTC) | 36.00 | 1.40 | 0.36 | 0.01 |
| Blue core composite (BIC) | 46.80 | 2.60 | 0.67 | 0.01 |

4. Discussion

The aim was to utilise both virgin and used textile fabrics due to their porous structures as a central element in the composites. Additionally, the textile was placed between two layers of facings, eliminating any potential contamination concerns.

Therefore, instead of simply discarding the materials by throwing them into the landfill, we have the opportunity to utilise them more effectively by incorporating them as reinforcement in the body of composites.

Compared to typical standard sandwich structures that utilise standard cores such as foams and balsa wood [18], it could be argued that the highest bending properties are not expected to be achieved with these types of constructed panels. However, these panels can still offer a good level of bending properties, particularly for less demanding applications such as semi-structural parts.

For the drop weight (impact) test, it is important to note that the maximum forces obtained from the sandwich composite specimens with PA cores in this research showed higher values compared to the previously mentioned ones found in the literature from the typical sandwich panels (the values obtained from the literature are compared with the findings from the current work in Section 3.2.1).

To evaluate the bonding between the skins and the textile material, it is recommended to observe the interface between the layers using microscope equipment. The microscope images of the control and sandwich composite specimens are shown in Figure 7. As can be seen in all the microscope images of the composites taken under the microscope, the bonding between the layers of the control specimen was excellent (Figure 7a), and is successful in all formulations. Figure 7b,c show the microscope pictures of VTC and VtC, respectively. The interface of these two sandwiches exhibits the virgin textile core, which is depicted as white in colour, and a layer of rayon fabric, which was successfully impregnated together. The interface between the layers is displayed in a red rectangle, and the thickness of the facing is presented by a red arrow. Similarly, the interface between the textile core and the rayon composite skin is depicted in Figure 7d,e, for the sandwich composites containing the end-of-life textiles. The bonding for BIC and BC composites was found to be excellent.

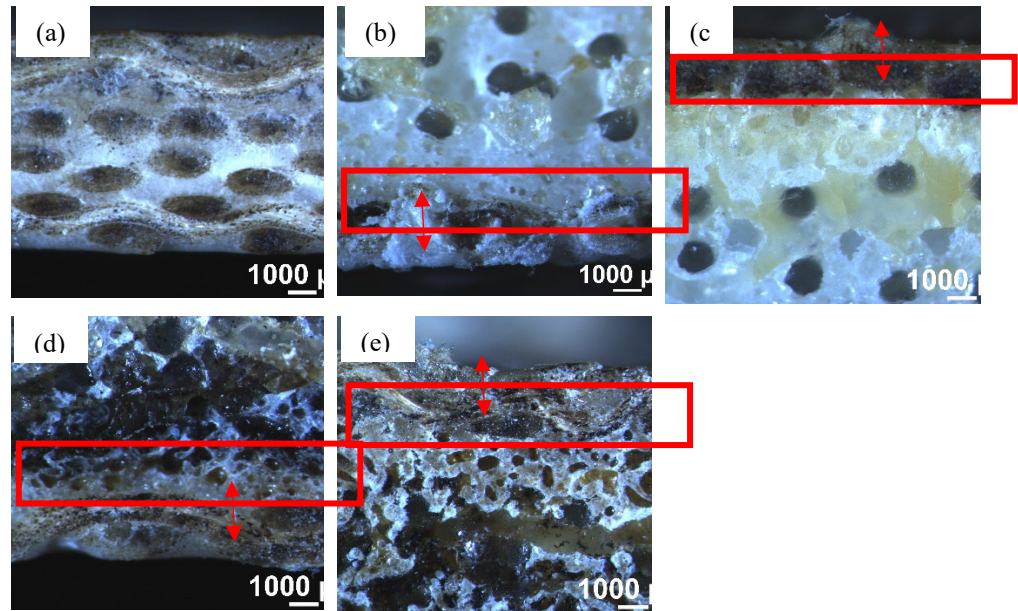


Figure 7. Microscopy images of (a) Control, (b) VTC, (c) VtC, (d) BIC, and (e) BC.

5. Conclusions

The sandwich composites containing regenerated cellulose fabric, bio-based PP composite skins, and recycled PA textiles were produced successfully using the hot press method. The aim was to utilise end-of-life textiles from industry and provide a secondary application for them. It was discovered that substituting these recycled textiles for rayon fabrics can maintain the mechanical performance of the composite laminate. In particular, due to the porosity and durability of these PA textiles, greater bending force and stiffness than those of control were achieved. For the LVI tests, the sandwich composites were found to reveal comparable LVI energy (ca. 28 J), maximum displacement (~13–14 mm), and peak force (in the range of 4.8–5.2 kN) with those of the control. A good agreement between the bending and impact test results in terms of displacement was observed. Force-wise, nearly the same trend was found for different sandwich composites (VTC > VtC, BC, BIC) as obtained from the flexural and drop impact tests. Tensile strength and modulus of sandwich composites were lower than those of control due to the porous structure of the textiles used as core materials and also the presence of more rayon fibers, which possess higher tensile properties than PA core, in the control composite. As observed in the visual inspection of the sandwich laminates, bio-based sandwich composite specimens containing the recycled cores showed larger microcracks than VTC and control. The CT images illustrated no fiber delamination, bundle breakage, or fiber bundle splitting after the drop test. These digital

and CT images evidenced good bonding between PA cores and bio-based PP composite skins. All the results obtained prove the potential of end-of-life textile materials for use in secondary applications, especially-composite associated components. This type of usage can lower the costs of composite fabrication while simultaneously providing sufficient mechanical properties. It can be concluded that the inclusion of used textiles can address both sustainable issues and cost-property benefits and eventually lead to low-cost, eco-friendly, and lightweight composite structures. It is interesting to investigate the effect of using end-of-life or waste textiles as reinforcement in natural fiber thermoset systems. Therefore, our future work will focus on studying these types of composites. Additionally, we will also examine other types of textile materials.

Author Contributions: Conceptualisation, P.K. and M.S.; methodology, P.K., H.N.D., S.H.D., A.F.G., M.D., and H.N.D.; validation, P.K. and M.S.; formal analysis, A.F.G. and P.K. investigation, A.F.G.; resources, M.S., H.N.D., and M.D.; data curation, A.F.G. and P.K.; writing—original draft preparation, A.F.G. and P.K.; writing—review and editing, P.K., M.S., and H.N.D.; visualisation, P.K. and M.S.; supervision, P.K.; project administration, P.K. and M.S.; funding acquisition, P.K. All authors have read and agreed to the published version of the manuscript.

Funding: This research was funded by VINNOVA, grant number 202202576, knowledge foundation (KK-stiftelsens), grant number 20200142, and ÅForsk foundation, grant number 20412. The APC was funded by University of Borås.

References

1. Lu, L.; Fan, W.; Meng, X.; Liu, T.; Han, L.; Zhang, T.; Dong, J.; Yuan, L.; Tian, H. Modal analysis of 3D needled waste cotton fiber/epoxy composites with experimental and numerical methods. *Text. Res. J.* 2021, 91, 358–372.
2. Weber, S.; Lynes, J.; Young, S.B. Fashion interest as a driver for consumer textile waste management: Reuse, recycle or disposal. *Int. J. Consum. Stud.* 2017, 41, 207–215.
3. Dissanayake, D.G.K.; Weerasinghe, D.; Wijesinghe, K.; Kalpage, K. Developing a compression moulded thermal insulation panel using postindustrial textile waste. *Waste Manag.* 2018, 79, 356–361.

4. Liu, X.; Tian, F.; Zhao, X.; Du, R.; Xu, S.; Wang, Y.-Z. Recycling waste epoxy resin as hydrophobic coating of melamine foam for high-efficiency oil absorption. *Appl. Surf. Sci.* 2020, 529, 147151.
5. Kang, G.-S.; Lee, G.; Cho, S.Y.; Joh, H.-I.; Lee, D.C.; Lee, S. Recycling of waste tires by synthesizing N-doped carbon-based catalysts for oxygen reduction reaction. *Appl. Surf. Sci.* 2021, 548, 149027.
6. Kalia, S.; Kaith, B.S.; Kaur, I. Pretreatments of natural fibers and their application as reinforcing material in polymer compo-sites—A review. *Polym. Eng. Sci.* 2009, 49, 1253–1272,.
7. del Mar Barbero-Barrera, M.; Pombo, O.; de los Angeles Navacerrada, M. Textile fibre waste bindered with natural hydraulic lime. *Compos. Part B Eng.* 2016, 94, 26–33.
8. Khalili, P.; Skrifvars, M.; Ertürk, A.S. Fabrication, Mechanical Testing and Structural Simulation of Regenerated Cellulose Fabric Elium® Thermoplastic Composite System. *Polymers* 2021, 13, 2969.
9. Johnson, R.K.; Zink-Sharp, A.; Renneckar, S.H.; Glasser, W.G. Mechanical properties of wetlaid lyocell and hybrid fi-ber-reinforced composites with polypropylene. *Compos. Part A Appl. Sci. Manuf.* 2008, 39, 470–477.
10. Franciszczak, P.; Merijs-Meri, R.; Kalniņš, K.; Błędzki, A.; Zicans, J. Short-fibre hybrid polypropylene composites reinforced with PET and Rayon fibres—Effects of SSP and interphase tailoring. *Compos. Struct.* 2017, 181, 121–137.
11. Khalili, P.; Tshai, K.Y.; Kong, I. Natural fiber reinforced expandable graphite filled composites: Evaluation of the flame re-tardancy, thermal and mechanical performances. *Compos. Part A Appl. Sci. Manuf.* 2017, 100, 194–205.
12. Khalili, P.; Blinzler, B.; Kádár, R.; Blomqvist, P.; Sandinge, A.; Bisschop, R.; Liu, X. Ramie fabric Elium® composites with flame retardant coating: Flammability, smoke, viscoelastic and mechanical properties. *Compos. Part A Appl. Sci. Manuf.* 2020, 137, 105986.
13. Khalili, P.; Kádár, R.; Skrifvars, M.; Blinzler, B. Impregnation behaviour of regenerated cellulose fabric Elium® composite: Experiment, simulation and analytical solution. *J. Mater. Res. Technol.* 2021, 10, 66–73.

14. Ganster, J.; Fink, H.-P.; Pinnow, M. High-tenacity man-made cellulose fibre reinforced thermoplastics—Injection moulding compounds with polypropylene and alternative matrices. *Compos. Part A Appl. Sci. Manuf.* 2006, 37, 1796–1804,.
15. Franciszczak, P.; Bledzki, A.K. Tailoring of dual-interface in high tenacity PP composites—Toughening with positive hybrid effect. *Compos. Part A Appl. Sci. Manuf.* 2016, 83, 185–192.
16. Karian, H. *Handbook of Polypropylene and Polypropylene Composites, Revised and Expanded*; CRC Press: Boca Raton, FL, USA, 2003.
17. Skrifvars, M.; Dhakal, H.; Zhang, Z.; Gentilcore, J.; Åkesson, D. Study on the mechanical properties of unsaturated polyester sandwich biocomposites composed of uniaxial warp-knitted and non-woven viscose fabrics. *Compos. Part A Appl. Sci. Manuf.* 2019, 121, 196–206.
18. Khalili, P.; Skrifvars, M.; Dhakal, H.N.; Jiang, C. Regenerated cellulose fabric reinforced bio-based polypropylene sandwich composites: Fabrication, mechanical performance and analytical modelling. *J. Mater. Res. Technol.* 2023, 22, 3423–3435.
19. Ude, A.U.; Ariffin, A.K.; Azhari, C.H. Azhari, Impact damage characteristics in reinforced woven natural silk/epoxy composite face-sheet and sandwich foam, coremat and honeycomb materials. *Int. J. Impact Eng.* 2013, 58, 31–38.
20. Oliveira, P.R.; May, M.; Kilchert, S.; de Oliveira, L.; Panzera, T.H.; Placet, V.; Scarpa, F.; Hiermaier, S. Eco-friendly panels made of autoclaved flax composites and upcycled bottle caps core: Experimental and numerical analysis. *Compos. Part C Open Access* 2021, 4, 100114.
21. Hachemane, B.; Zitoune, R.; Bezzazi, B.; Bouvet, C. Sandwich composites impact and indentation behaviour study. *Compos. Part B Eng.* 2013, 51, 1–10.
22. Zhang, D.; Gu, Y.; Zhang, Z.; Jia, M.; Yue, S.; Li, G. Effect of off-axis angle on low-velocity impact and compression after impact damage mechanisms of 3D woven composites. *Mater. Des.* 2020, 192, 108672.

23. Sun, M.; Liu, X.; Zhang, D.; Sun, J.; Qian, K. Effects of structural defects on low-velocity impact damage mechanisms of three-dimensional braided composites based on X-ray micro-computed tomography. *Polym. Test.* 2021, 104, 107403.